

AD-A077 032

ROME AIR DEVELOPMENT CENTER GRIFFISS AFB NY
MODES OF DIELECTRIC WAVEGUIDES OF ARBITRARY CROSS-SECTIONAL SHA--ETC(U)
JUN 79 L EYGES , P GIANINO , P WINTERSTEINER

F/G 9/3

UNCLASSIFIED

RADC-TR-79-197

NL

1 OF 1
AD
A077032



END
DATE
FILMED
12 79
DDC

AD A 077032

RADC-TR-79-197
In-House Report
June 1979

LEVEL *14*



MODES OF DIELECTRIC WAVEGUIDES OF ARBITRARY CROSS-SECTIONAL SHAPE

LEONARD EYGES
PETER GIANINO

ARCON Corporation, 260 Bear Hill Road, Waltham, Massachusetts 02154
P. Wintersteiner

APPROVED FOR PUBLIC RELEASE; DISTRIBUTION UNLIMITED

DDC
FORM
NOV 21 1979
REGULIT
E

DDC FILE COPY

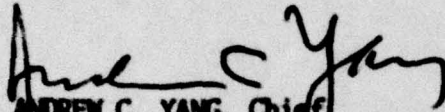
ROME AIR DEVELOPMENT CENTER
Air Force Systems Command
Griffiss Air Force Base, New York 13441

79 11 19 123

This report has been reviewed by the RADC Information Office (OI) and is releasable to the National Technical Information Service (NTIS). At NTIS it will be releasable to the general public, including foreign nations.

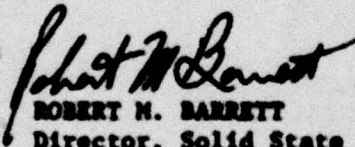
RADC-TR-79-197 has been reviewed and is approved for publication.

APPROVED:



ANDREW C. YANG, Chief
Electro-Optic Device Technology Branch
Solid State Sciences Division

APPROVED:



ROBERT M. BARRETT
Director, Solid State Sciences Division

FOR THE COMMANDER:



JOHN P. HUSS
Acting Chief, Plans Office

If your address has changed or if you wish to be removed from the RADC mailing list, or if the addressee is no longer employed by your organization, please notify RADC (ESO), Hanscom AFB MA 01731. This will assist us in maintaining a current mailing list.

Do not return this copy. Retain or destroy.

Unclassified

SECURITY CLASSIFICATION OF THIS PAGE (When Data Entered)

REPORT DOCUMENTATION PAGE		READ INSTRUCTIONS BEFORE COMPLETING FORM
1. REPORT NUMBER RADC-TR-79-197	2. GOVT ACCESSION NO.	3. RECIPIENT'S CATALOG NUMBER
4. TITLE (and Subtitle) MODES OF DIELECTRIC WAVEGUIDES OF ARBITRARY CROSS-SECTIONAL SHAPE	5. TYPE OF REPORT & PERIOD COVERED In-House Report June 1979	
6. AUTHOR(s) Leonard Byges, Peter Giamino, P. Wintersteiner	7. PERFORMING ORG. REPORT NUMBER N/A	
8. PERFORMING ORG. NAME AND ADDRESS Deputy for Electronic Technology (RADC/ESO) Hanscom AFB Massachusetts 01731	9. CONTRACT OR GRANT NUMBER(s) N/A	
10. CONTROLLING OFFICE NAME AND ADDRESS Deputy for Electronic Technology (RADC/ESO) Hanscom AFB Massachusetts 01731	11. PROGRAM ELEMENT PROJECT, TASK AREA & WORK UNIT NUMBERS 61102F 2306205	
12. MONITORING AGENCY NAME & ADDRESS (if different from Controlling Office) Same	13. REPORT DATE June 79	
14. DISTRIBUTION STATEMENT (of this Report) Approved for public release; distribution unlimited.	15. SECURITY CLASS. (of this report) Unclassified	
16. DISTRIBUTION STATEMENT (of the abstract entered in Block 20, if different from Report) Same	17. SECURITY CLASS. (of this abstract) Unclassified	
18. SUPPLEMENTARY NOTES * ARCON Corp., 260 Bear Hill Road, Waltham, MA 02154		
19. KEY WORDS (Continue on reverse side if necessary and identify by block number) Optical waveguides Waveguide propagation Fiber optics Waveguide modes		
20. ABSTRACT (Continue on reverse side if necessary and identify by block number) An integral representation technique is presented for determining the modal propagation properties of a homogeneous cylindrical dielectric waveguide of arbitrary cross-sectional shape and index n_1 embedded in a medium of index n_2 . Results are given for weakly guiding fibers of various shapes. Among these are rectangles and ellipses, which makes comparisons with previous work possible.		

DD FORM 1 JAN 73 1473 EDITION OF 1 NOV 65 IS OBSOLETE

Unclassified

SECURITY CLASSIFICATION OF THIS PAGE (When Data Entered)

309 050

set

Summary

A technique is presented for determining the modal propagation properties of a homogeneous cylindrical dielectric waveguide of arbitrary cross-sectional shape and index n_1 embedded in a medium of index n_2 . For the cylinder parallel to the z -axis all field components can be derived from E_z and B_z . Integral representations for E_z and B_z are derived which satisfy the appropriate Helmholtz equations inside and outside the guide and which guarantee that the boundary conditions are satisfied. On expanding E_z and B_z in certain sets of basis functions the integral representations become a set of linear equations. The vanishing of the determinant of this set yields the propagation constants of the various modes. For the important special case of weakly guiding fibers ($n_1 \approx n_2$), E_z and B_z become small and we deal instead with the relatively large transverse rectangular components of \underline{E} and \underline{B} , any one of which satisfies a Helmholtz equation inside and outside the guide. As with the general case, an integral representation is derived, basis functions are inserted, and a determinantal equation is generated whose roots yield the modal propagation constants. Results are given for weakly guiding fibers of various shapes. Among these are rectangles and ellipses, which makes comparisons with previous work possible.

Accession For	
NTIS GRA&I	<input checked="checked" type="checkbox"/>
DDC TAB	<input type="checkbox"/>
Unannounced	<input type="checkbox"/>
Justification	
By _____	
Distribution/ _____	
Availability Codes	
Dist	Avail and/or special
A	

Contents

1. INTRODUCTION	9
2. INTEGRAL REPRESENTATIONS FOR THE WEAKLY GUIDING CASE	11
3. EQUIVALENT SETS OF LINEAR EQUATIONS	15
4. INTEGRAL REPRESENTATIONS FOR WEAKLY GUIDING FIBERS: $n_1 \neq n_2$	19
5. SYMMETRY CONSIDERATIONS	21
6. EQUATIONS FOR THE WEAKLY GUIDING CASE	23
7. COMPUTATIONAL TECHNIQUES	25
8. RESULTS AND COMPARISON WITH OTHER WORK	28
8.1 Rectangular Cross Sections	29
8.2 Elliptical Cross Sections	36
8.3 Other Shapes	41
8.4 "Evolution" of the Modes	42
8.5 Comparison With Other Work	48
9. CONCLUSION	50
REFERENCES	51

Illustrations

1. Cross Section of a Cylindrical Dielectric Guide Parallel to the z-Axis	11
2. Plot of the Function $\rho(\phi)$ Given in Equation (60) for $0 \leq \phi \leq \pi/2$ Only, $\tilde{R} = 1$, and Various Values of N	28
3. Modes of the Weakly Guiding Square Guide	30
4. Modes of the Weakly Guiding Rectangular Guide with $\tilde{R} = 1, 2$	30
5. Modes of the Weakly Guiding Rectangular Guide with $\tilde{R} = 1, 5$	31
6. Modes of the Weakly Guiding Rectangular Guide with $\tilde{R} = 2$	31
7. Field Intensity as a Function of ρ/b for the R_1^I Mode of a Square Guide with $\beta = 3$	33
8. Field Intensity as a Function of ρ/b for the R_4^I Mode of the Square Guide with $\beta = 3$ and Various Values of ϕ	35
9. Modes of the Weakly Guiding Circular Guide	38
10. Modes of the Weakly Guiding Elliptical Guide with $\tilde{R} = 1, 2$	38
11. Modes of the Weakly Guiding Elliptical Guide with $\tilde{R} = 1, 5$	39
12. Modes of the Weakly Guiding Elliptical Guide with $\tilde{R} = 2$	39
13. Modes of the Weakly Guiding Superelliptical Guide with $\tilde{R} = 1, N = 2$	41
14. Modes of the Weakly Guiding Superelliptical Guide with $\tilde{R} = 1, N = 5$	41
15. Modes of the Weakly Guiding Cusp-Shaped Guide with $\tilde{R} = 1, N = 0.3$	42
16. The R_2^I Mode of the Weakly Guiding Rectangular Guide as \tilde{R} Changes from 1 to 2	43
17. The R_1^{II} Mode of the Weakly Guiding Rectangular Guide as \tilde{R} Changes from 1 to 10	43
18. The R_1^{IV} Mode of the Weakly Guiding Rectangular Guide as \tilde{R} Changes from 1 to 2	44
19. The R_1^I Mode of the Weakly Guiding Rectangular Guide as \tilde{R} Changes from 1 to ∞	44
20. The R_1^{III} Mode of the Weakly Guiding Rectangular Guide as \tilde{R} Changes from 1 to 2	45
21. Variation of P^2 with Change in Aspect Ratio for the First Five Modes of the Weakly Guiding Rectangular Guide at Two Values of β	45
22. Variation of P^2 with Change in Aspect Ratio for Some of the First Few Modes of the Weakly Guiding Elliptical Guide at Two Values of β	47

Tables

1. Results for the Dominant (Noncutoff) R_1^I Mode of the Weakly Guiding Square Guide	32
2. Values of the Propagation Constant, P^2 , for $\beta = 2$ for the First 13 Modes of a Square Guide, Obtained with Determinants up to Order 4	34
3. Results for the Dominant (Noncutoff) R_1^I Mode of the Weakly Guiding 2:1 Rectangular Guide	36
4. Results for the First 13 Modes of the 2:1 Rectangular Guide, Ordered According to the Value of β at Cutoff	37
5. Values of β at Cutoff for Elliptical Guides with Different Aspect Ratios and for a Rectangular Guide with $R = 2$	40

Modes of Dielectric Waveguides of Arbitrary Cross - Sectional Shape

1. INTRODUCTION

With the increased interest in fiber optic or integrated optic communication techniques has come a need to know in increasing detail the propagation properties of cylindrical dielectric waveguides (Gloge,¹ Goell,² Marcatili³). In fact, the literature has so burgeoned that it would be excessive to try to quote all the individual papers that discuss the subject. Happily, there are by now several excellent books and review articles that make this unnecessary (Marcuse,⁴ Kapany and Burke⁵).

The problem of electromagnetic propagation down a dielectric cylinder is closely related to the problem of scattering of electromagnetic waves from the same cylinder. It is then not surprising that methods used for the scattering problem (Eyges⁶) have also been applied to the problem of propagation. Thus,

(Received for publication 3 July 1979)

1. Gloge, D. (1971) Appl. Opt. 10:2252.
2. Goell, J. E. (1969) Bell Sys. Tech. J. 48:2133.
3. Marcatili, E. A. J. (1969) Bell Sys. Tech. J. 48:2071.
4. Marcuse, D. (1974) Theory of Dielectric Optical Waveguides, Academic Press, N. Y.
5. Kapany, N. S. and Burke, J. J. (1972) Optical Waveguides, Academic Press, N. Y.
6. Eyges, L. (1973) Ann. Phys. 81:567.

point matching (Goell²) and ray tracing (Love and Snyder; de Vita⁷) techniques have been applied. Despite much work, however, there is no one general analytic method which applies to single guides of arbitrary cross-sectional shape and to the coupling between two or more such guides.

In this paper we present such a method for single guides; its extension to coupled guides is in preparation. The method is largely analytic although finally machine computation is required. The method not only provides new techniques for irregularly shaped guides, but also has the minor advantage of providing neat derivations of the standard formulae for single circular guides, including the well-known approximations that arise when the index of refraction is little different from that of the surrounding medium. The present method is an extension of recent new techniques for solving the problem of scattering by irregularly shaped dielectric bodies, and in the static limit, for solving the problem of an irregular dielectric or permeable body in an external field (Eyges,⁶ Eyges and Gianino,⁸ Nelson and Eyges⁹). The general idea here is the same as in those papers. That is, an integral representation for the various field components is derived that is equivalent to the appropriate differential equations inside and outside the guide and that guarantees as well that the various boundary conditions are satisfied. These differential equations for the field components inside the guide have a set of known solutions that can be considered as a set of basis functions. The field components can be expanded in a series of these basis functions, with unknown coefficients. On introducing the expansions into the integral representations, they become a set of linear (matrix) equations whose matrix elements involve these basis functions in line integrals that are taken over the boundary of the cross-sectional shape. This is the only way the boundary enters; there is no need to match interior and exterior solutions across it. Since the set of matrix equations is a homogeneous one, it has solutions only for certain allowed values of the parameters involved. One of these parameters is the propagation constant we seek.

The description above applies to a guide of index n_1 embedded in a medium of smaller index n_2 but with no other restrictions on the magnitudes of n_1 and n_2 . In practice however, it is very common for n_1 to be close to n_2 . In this "weakly guiding" case certain vectorial aspects of the general procedure outlined above become simpler, and, in fact, the problem can be reduced in a good approximation to a scalar one. We have therefore concentrated on this scalar formulation and have based our numerical calculations on it.

7. Love, J. D. and Snyder, A. W. (1977) Ann. Telecommunications 32:109;
de Vita, P. (1977) Ann. Telecommunications 32:115.
8. Eyges, L. and Gianino, P. D. (1979) IEEE Trans. Ant. & Prop. AP-27:557.
9. Nelson, A. E. and Eyges, L. (1976) J. Opt. Soc. Am. 66:254.

2. INTEGRAL REPRESENTATIONS FOR THE WEAKLY GUIDING CASE

In this section integral representations in the weakly guiding case are derived for the cylindrical guide of arbitrary cross section sketched in Figure 1. The time dependence is given as $e^{-i\omega t}$, so that, for example, the electric field $\underline{E}(\underline{r}, t)$ is written as $\underline{E} = \underline{E}_{\omega} e^{-i\omega t}$. The guide medium is assumed uniform with index of refraction n_1 and dielectric constant ϵ_1 , related by $n_1^2 = \epsilon_1$ and similarly the external medium is characterized by $n_2^2 = \epsilon_2$. Then \underline{E}_{ω} (similarly \underline{B}_{ω}) satisfies $(\nabla^2 + k_1^2) \underline{E}_{\omega} = 0$ inside the guide and $(\nabla^2 + k_2^2) \underline{E}_{\omega} = 0$ in the external medium, where $k_1 = n_1 k_0$, $k_2 = n_2 k_0$ and $k_0 = \omega/c$.

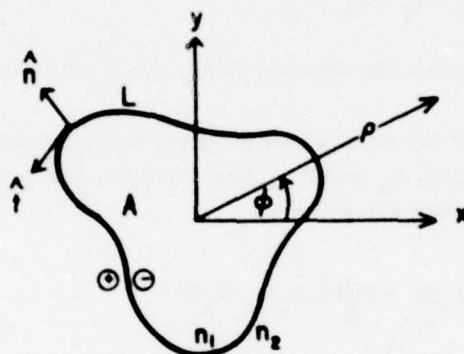


Figure 1. Cross Section of a Cylindrical Dielectric Guide Parallel to the z -Axis. The cross-sectional area is denoted by A , its bounding curve by L , the outward normal to the cylinder is \hat{n} , and the unit vector tangent to L is \hat{t} . The positive z -axis is out of the plane of the paper

For solutions that correspond to wave propagation along the guide, it will be assumed that the only z -dependence is $e^{ik_g z}$.

$$\left. \begin{array}{l} \underline{E}_{\omega}(\underline{r}) \\ \underline{B}_{\omega}(\underline{r}) \end{array} \right\} = \left. \begin{array}{l} \underline{E}(\underline{\rho}) \\ \underline{B}(\underline{\rho}) \end{array} \right\} e^{ik_g z} \quad (1)$$

where $\underline{\rho}$ is a vector in the plane perpendicular to the z -axis and k_g is the propagation constant in the z -direction. It follows that $\underline{E}(\underline{\rho})$ and $\underline{B}(\underline{\rho})$ satisfy

$$(\nabla_1^2 + \gamma_1^2) \begin{pmatrix} \underline{E}(\rho) \\ \underline{B}(\rho) \end{pmatrix} = 0 \text{ inside the guide} \quad (2)$$

$$(\nabla_1^2 - \gamma_2^2) \begin{pmatrix} \underline{E}(\rho) \\ \underline{B}(\rho) \end{pmatrix} = 0 \text{ outside the guide} \quad (3)$$

where ∇_1^2 is the two-dimensional Laplacian and

$$\gamma_1^2 = k_1^2 - k_g^2 \quad ; \quad \gamma_2^2 = k_g^2 - k_2^2 \quad (4)$$

Eq. (3) reflects the fact that the external fields decay with increasing distance from the guide.

It is well known that for the present problem the transverse components of \underline{E} and \underline{B} are derivable from E_z and B_z . For example, the perpendicular components E_\perp inside the medium are given by

$$\underline{E}_\perp = \frac{i}{\epsilon_1 k_0^2 - k_g^2} [k_0 (\nabla_\perp \times \underline{B}_z) + k_g (\nabla_\perp E_z)]$$

On forming the transverse tangential component E_t by dotting this with $\hat{t} = \hat{z} \times \hat{n}$ and doing the same for B_t we find

$$E_t = \frac{i}{\gamma_1^2} \left(k_g \frac{\partial E_z}{\partial t} - k_0 \frac{\partial B_z}{\partial n} \right) \quad (5)$$

$$B_t = \frac{i}{\gamma_1^2} \left(k_g \frac{\partial B_z}{\partial t} + \epsilon_1 k_0 \frac{\partial E_z}{\partial n} \right) \quad (6)$$

Similar formulae hold outside the guide, with ϵ_1 and γ_1^2 replaced by ϵ_2 and $-\gamma_2^2$ respectively.

We want to derive integral equations for E_z and B_z and want these equations to incorporate the boundary conditions, which are that the tangential components of both \underline{E} and \underline{B} be continuous across the boundary curve L . These tangential components are the longitudinal E_z and B_z and the transverse E_t and B_t . To get the required integral representation we follow a procedure very similar to that in

a previous paper by Eyges.⁶ It is easy to find an integral representation for E_z which satisfies Eqs. (2) and (3) and also guarantees that E_z be continuous. This is

$$E_z(\underline{\rho}) = -(\gamma_1^2 + \gamma_2^2) \int E_z(\underline{\rho}') g_{\gamma_2}(\underline{\rho}, \underline{\rho}') dA' \quad (7)$$

where the two-dimensional Green function satisfies

$$(\nabla_1^2 - \gamma_2^2) g_{\gamma_2}(\underline{\rho}, \underline{\rho}') = \delta(\underline{\rho} - \underline{\rho}') \quad (8)$$

There is, of course, a similar equation, with similar properties, for B_z . However, these equations do not satisfy the conditions that E_t and B_t be continuous. The reason they do not is that the condition of the continuity of E_t and B_t can be rephrased as a condition on the discontinuity across the boundary of $\partial E_z / \partial n$ and $\partial B_z / \partial n$ (jump condition), whereas Eq. (7) implies that E_z is continuous, and the similar equation implies that B_z is continuous. But Eq. (7) can be modified, much as in the previous work on scattering, by the addition to it of certain line integrals that guarantee that the jump condition be satisfied, and we shall do just this.

To get the jump conditions we use Eq. (5) for E_t just inside the boundary (subscript -) and equate it to its counterpart for E_t just outside the boundary (subscript +) to find

$$\frac{1}{\gamma_1^2} \left(k_g \frac{\partial E_z}{\partial t} - k_o \frac{\partial B_z}{\partial n} \right)_- = \frac{1}{\gamma_2^2} \left(-k_g \frac{\partial E_z}{\partial t} + k_o \frac{\partial B_z}{\partial n} \right)_+ \quad (9)$$

Now since E_z is continuous across the boundary so is $\partial E_z / \partial t$ so we do not need subscripts + and - on it. Thus, Eq. (9) becomes a condition on the discontinuity of the normal derivative of B_z :

$$\left. \frac{\partial B_z}{\partial n} \right|_+ - \left. \frac{\partial B_z}{\partial n} \right|_- = - \left(\frac{\gamma_2^2}{\gamma_1^2} + 1 \right) \left. \frac{\partial B_z}{\partial n} \right|_- + \frac{k_g}{k_o} \left(\frac{\gamma_2^2}{\gamma_1^2} + 1 \right) \frac{\partial E_z}{\partial t} \quad (10)$$

In much the same way, the continuity condition on B_t becomes one on the discontinuity of the normal derivative of E_z :

$$\left. \frac{\partial E_z}{\partial n} \right|_+ - \left. \frac{\partial E_z}{\partial n} \right|_- = - \left(\frac{\epsilon_1 \gamma_2^2}{\epsilon_2 \gamma_1^2} + 1 \right) \left. \frac{\partial E_z}{\partial n} \right|_- - \frac{k_g}{\epsilon_2 k_o} \left(\frac{\gamma_2^2}{\gamma_1^2} + 1 \right) \frac{\partial B_z}{\partial t} \quad (11)$$

To exploit these results, we recall some properties of the following line integral over the boundary, a function of $\underline{\rho}$ we designate by $\xi(\underline{\rho})$:

$$\xi(\underline{\rho}) = \int_L g_{\gamma_2}(\underline{\rho}, \underline{\rho}') \sigma(\underline{\rho}') dL' \quad (12)$$

where σ is for the moment an arbitrary function. It is well known that $\xi(\underline{\rho})$ is continuous across the boundary but has discontinuous normal derivatives

$$\left. \frac{\partial \xi}{\partial n} \right|_+ - \left. \frac{\partial \xi}{\partial n} \right|_- = \sigma(\underline{\rho}) \quad (13)$$

where $\underline{\rho}$ on the right hand side of Eq. (13) is, of course, on the boundary. Now we add to the provisional Eq. (7) for E_z a line integral like Eq. (12) but with $\sigma(\underline{\rho})$ taken to be the function on the right hand side of Eq. (11), to get:

$$\begin{aligned} E_z(\underline{\rho}) = & -(\gamma_1^2 + \gamma_2^2) \int_A E_z(\underline{\rho}') g_{\gamma_2}(\underline{\rho}, \underline{\rho}') dA' - \frac{1}{\epsilon_2 \gamma_1^2} \int_L \left\{ (\epsilon_1 \gamma_2^2 + \epsilon_2 \gamma_1^2) \left. \frac{\partial E_z}{\partial n'} \right|_- \right. \\ & \left. + \frac{k}{k_0} (\gamma_2^2 + \gamma_1^2) \frac{\partial B_z}{\partial t'} \right\} g_{\gamma_2}(\underline{\rho}, \underline{\rho}') dL' \quad (14) \end{aligned}$$

This is now the final desired equation for E_z . It still satisfies Eqs. (2) and (3), guarantees the continuity of E_z , and, in addition, by virtue of the line integral in it and Eq. (13), now satisfies the jump condition Eq. (11), i.e., the condition on the continuity of B_t . The equation for B_z , derived similarly, is

$$\begin{aligned} B_z(\underline{\rho}) = & -(\gamma_1^2 + \gamma_2^2) \int_A B_z(\underline{\rho}') g_{\gamma_2}(\underline{\rho}, \underline{\rho}') dA' - \frac{\gamma_1^2 + \gamma_2^2}{\gamma_1^2} \int_L \left(\left. \frac{\partial B_z}{\partial n'} \right|_- - \frac{k}{k_0} \frac{\partial E_z}{\partial t'} \right) \\ & g_{\gamma_2}(\underline{\rho}, \underline{\rho}') dL' \quad (15) \end{aligned}$$

For many purposes it is convenient to transform Eqs. (14) and (15) by replacing the area integrals with line integrals. Thus, in Eq. (14) in the integral over A we can use $-\gamma_2^2 g_{\gamma_2} = \delta(\underline{\rho} - \underline{\rho}') - \nabla_1^2 g_{\gamma_2}$ and $-\gamma_1^2 E_z = \nabla_1^2 E_z$ and rewrite it as follows:

$$\begin{aligned}
& -(\gamma_1^2 + \gamma_2^2) \int_A E_z g_{\gamma_2} dA' = \int_A (\delta(\rho - \rho') - \nabla_1^2 g_{\gamma_2}) E_z dA' + \int_A \nabla_1^2 E_z g_{\gamma_2} dA' \\
& = E_z + \int_L \left(g_{\gamma_2} \frac{\partial E_z}{\partial n} - E_z \frac{\partial g_{\gamma_2}}{\partial n} \right) dL' \quad (\rho \text{ inside guide}) \quad (16)
\end{aligned}$$

where we have used Green's second identity in deriving the last equation from its predecessor. With Eq. (16) in Eq. (14) we find after cancelling some terms:

$$\begin{aligned}
0 = & - \int_L E_z \frac{\partial g_{\gamma_2}}{\partial n'} dL' - \frac{\epsilon_1 \gamma_2^2}{\epsilon_2 \gamma_1^2} \int_L g_{\gamma_2} \frac{\partial E_z}{\partial n'} \Big|_- dL' - \frac{1}{\epsilon_2 \gamma_1^2} \frac{k_g}{k_o} (\gamma_1^2 + \gamma_2^2) \\
& \int_L \frac{\partial B_z}{\partial t'} g_{\gamma_2} dL' \quad (17)
\end{aligned}$$

In much the same way, Eq. (15) becomes

$$\begin{aligned}
0 = & - \int_L B_z \frac{\partial g_{\gamma_2}}{\partial n'} dL' - \frac{\gamma_2^2}{\gamma_1^2} \int_L \frac{\partial B_z}{\partial n'} \Big|_- g_{\gamma_2} dL' + \frac{k_g}{k_o} \left(\frac{\gamma_1^2 + \gamma_2^2}{\gamma_1^2} \right) \\
& \int_L \frac{\partial E_z}{\partial t'} g_{\gamma_2} dL' \quad (18)
\end{aligned}$$

These are the basic integral representations of the theory.

3. EQUIVALENT SETS OF LINEAR EQUATIONS

In this section the pair of integral Eqs. (17) and (18), is reduced to an equivalent pair of sets of linear algebraic equations by evaluating them at small ρ , much as was done in previous related work of Eyges.⁶ We assume that ρ is much less than the smallest value of ρ' that appears in the integrands of Eqs. (17) and (18). We can assure that this is possible by choosing the origin of the coordinate system in Figure 1 appropriately. Then, for use in Eqs. (17) and (18) we have the Green function expansion

$$g_{\gamma_2}(\rho, \rho') = \frac{-i}{4} \sum_{l=-\infty}^{\infty} J_l(\gamma_2 \rho) H_l(i\gamma_2 \rho') e^{il(\phi - \phi')} \quad (19)$$

whence

$$\frac{\partial g_{\gamma_2}}{\partial n'} = \frac{-i}{4} \sum_{l=-\infty}^{\infty} J_l(\gamma_2 \rho) e^{il\phi} \frac{\partial}{\partial n'} (H_l(i\gamma_2 \rho') e^{-il\phi'}) \quad (20)$$

If Eqs. (19) and (20) are inserted into Eqs. (17) and (18), there results, on dropping the common factor $-(i/4)J_l(\gamma_2 \rho)$

$$\int_L \left\{ E_z(\rho') \frac{\partial}{\partial n'} (H_l(i\gamma_2 \rho') e^{-il\phi'}) + \left[\frac{\epsilon_1 \gamma_2^2}{\epsilon_2 \gamma_1^2} \frac{\partial E_z}{\partial n'} + \frac{k_g}{\epsilon_2 k_0} \left(1 + \frac{\gamma_2^2}{\gamma_1^2} \right) \frac{\partial B_z}{\partial t'} \right] H_l(i\gamma_2 \rho') e^{-il\phi'} \right\} dL' = 0 \quad (21)$$

$$\int_L \left\{ B_z(\rho') \frac{\partial}{\partial n'} (H_l(i\gamma_2 \rho') e^{-il\phi'}) + \left[\frac{\gamma_2^2}{\gamma_1^2} \frac{\partial B_z}{\partial n'} - \frac{k_g}{k_0} \left(1 + \frac{\gamma_2^2}{\gamma_1^2} \right) \frac{\partial E_z}{\partial t'} \right] H_l(i\gamma_2 \rho') e^{-il\phi'} \right\} dL' = 0 \quad (22)$$

Now Eqs. (21) and (22) are reduced to sets of linear equations by expanding $E_z(\rho')$ and $B_z(\rho')$ in the sets of basis functions $J_s(\gamma_1 \rho) \cos s\phi$, $J_s(\gamma_1 \rho) \sin s\phi$, or $J_s(\gamma_1 \rho) e^{is\phi}$. For the moment, the exponential form is more convenient, so we write:

$$E_z(\rho') = \sum_{s=-\infty}^{\infty} A_s J_s(\gamma_1 \rho') e^{is\phi'} \quad (23)$$

$$B_z(\rho') = \sum_{s=-\infty}^{\infty} B_s J_s(\gamma_1 \rho') e^{is\phi'} \quad (24)$$

We shall assume that the normal \hat{n} is expressed in cylindrical coordinates,

$$\hat{n} = \hat{\rho} n_{\rho} + \hat{\phi} n_{\phi} \quad (25)$$

although, it can be advantageous, particularly with a cylinder whose cross section is a polygon, to express \hat{n} in Cartesian coordinates. In cylindrical coordinates, for a contour L that is defined by $\rho = \rho(\phi)$, one has:

$$n_{\rho} = \rho / \frac{dL}{d\phi} \quad , \quad n_{\phi} = - \frac{d\rho/d\phi}{dL/d\phi} \quad (26)$$

where

$$dL = \sqrt{\rho^2 + (d\rho/d\phi)^2} d\phi \quad (27)$$

Given Eqs. (23) and (24), the various quantities that enter Eqs. (21) and (22) are

$$\frac{\partial B_z(\rho')}{\partial n'} = \hat{n}' \cdot \nabla' B_z(\rho') = \left(\frac{dL'}{d\phi'} \right)^{-1} \sum_{s=-\infty}^{\infty} B_s e^{is\phi'} \left\{ \gamma_1 \rho' J_s'(\gamma_1 \rho') - \frac{is}{\rho'} \frac{\partial \rho'}{\partial \phi'} J_s(\gamma_1 \rho') \right\}$$

and similarly for E_z . For $\partial B_z / \partial t'$ we have, with $\hat{t}' = \hat{z}' \times \hat{n}'$

$$\begin{aligned} \frac{\partial B_z(\rho')}{\partial t'} &= (\hat{z}' \times \hat{n}') \cdot \nabla' B_z(\rho') = n_{\phi}' \frac{\partial B_z}{\partial \rho'} - \frac{n_{\rho}'}{\rho'} \frac{\partial B_t}{\partial \phi'} \\ &= \left(\frac{dL'}{d\phi'} \right)^{-1} \sum_{s=-\infty}^{\infty} B_s e^{is\phi'} \left\{ \gamma_1 J_s'(\gamma_1 \rho') \frac{\partial \rho'}{\partial \phi'} + is J_s(\gamma_1 \rho') \right\} \end{aligned}$$

These results are put into Eqs. (21) and (22) and the integration is converted to one over $d\phi'$ via $dL' = (dL'/d\phi')d\phi'$, whereupon these equations become:

$$\sum_{s=-\infty}^{\infty} \left\{ A_s \left(M_{Is} + \frac{\epsilon_1 \gamma_2^2}{\epsilon_2 \gamma_1^2} N_{Is} \right) + \frac{B_s}{\epsilon_2} Q_{Is} \right\} = 0 \quad (28)$$

$$\sum_{s=-\infty}^{\infty} \left\{ -A_s Q_{ls} + B_s \left(M_{ls} + \frac{\gamma_2^2}{\gamma_1^2} N_{ls} \right) \right\} = 0 \quad l = 0, \pm 1, \pm 2, \dots \quad (29)$$

where

$$\begin{aligned} M_{ls} &= \int_0^{2\pi} e^{i(s-l)\phi'} J_s(\gamma_1 \rho') \left[i\gamma_2 \rho' H_l(i\gamma_2 \rho') - \frac{il}{\rho'} \left(\frac{d\rho'}{d\phi'} \right) H_l(i\gamma_2 \rho') \right] d\phi' \\ N_{ls} &= \int_0^{2\pi} e^{i(s-l)\phi'} H_l(i\gamma_2 \rho') \left[\gamma_1 \rho' J_s'(\gamma_1 \rho') - \frac{is}{\rho'} \frac{\partial \rho'}{\partial \phi'} J_s(\gamma_1 \rho') \right] d\phi' \\ Q_{ls} &= \frac{k_g}{k_0} \left(1 + \frac{\gamma_2^2}{\gamma_1^2} \right) \int_0^{2\pi} e^{i(s-l)\phi'} H_l(i\gamma_2 \rho') \left[\gamma_1 J_s'(\gamma_1 \rho') \frac{\partial \rho'}{\partial \phi'} + is J_s(\gamma_1 \rho') \right] d\phi'. \end{aligned} \quad (30)$$

The homogeneous set of Eqs. (28) and (29) has solutions only if the determinant vanishes. Then the various roots of this vanishing determinant yield the propagation constants of the different modes of the guide.

Eqs. (28) and (29) can be applied to circular guides (radius a) to obtain results that are of course not new, but which do serve as a useful check on our procedure. For a circular guide $\partial \rho / \partial \phi = 0$ and all the off-diagonal matrix elements are zero, that is,

$$M_{ls} = 2\pi i\gamma_2 a J_l(\gamma_1 a) H_l'(i\gamma_2 a) \delta_{ls} \quad (31)$$

$$N_{ls} = -2\pi(\gamma_2^2 a / \gamma_1) J_l'(\gamma_1 a) H_l(i\gamma_2 a) \delta_{ls} \quad (32)$$

$$Q_{ls} = 2\pi(k_g/k_0)(1 + \gamma_2^2/\gamma_1^2) i l J_l(\gamma_1 a) H_l(i\gamma_2 a) \delta_{ls}. \quad (33)$$

If we let $x = \gamma_2 a$ and $y = \gamma_1 a$ in Eqs. (31) to (33), substitute these expressions into Eqs. (28) and (29), and then eliminate the A_l and B_l between these two equations, we get the standard dispersion relation (Marcuse⁴):

$$[(\epsilon_1 k_0^2/y)(-J'_I(y)/J_I(y)) - (\epsilon_2 k_0^2/x)(H'_I(i x)/H_I(i x))] \times \\ [J'_I(y)/y J_I(y) - H'_I(i x)/x H_I(i x)] = i^2 k_g^2 (y^2 - x^2)^2 / x^4 y^4. \quad (34)$$

4. INTEGRAL REPRESENTATIONS FOR WEAKLY GUIDING FIBERS: $n_1 \approx n_2$

An important practical case occurs when $n_1 \approx n_2$ so that the fiber is "weakly guiding." For circular fibers Gloge¹ has shown how the conventional treatment can be simplified. His essential point is that the longitudinal components E_z and B_z become small compared to the transverse components E_\perp , B_\perp and in fact $E_z/E_\perp \approx \sqrt{n_1 - n_2}$; the same for B_z/B_\perp . A similar result holds for the modes of the slab guide. It is clear, and we shall verify this below, that Gloge's arguments can be also applied to weakly guiding fibers of arbitrary cross-sectional shape. It then becomes more convenient to abandon the treatment of Section 3 in terms of E_z and B_z and to deal directly with the nonvanishing transverse fields E_\perp and B_\perp .

We want then to obtain integral representations for E_\perp and B_\perp analogous to those of Section 3 for E_z and B_z . To set up these latter integral representations, we had to take into account the continuity properties of their normal derivatives across the boundary. Similarly, in setting up the integral representations for E_\perp and B_\perp we must again inquire into the possibility of boundary discontinuities. To begin, we observe that the tangential components of E_\perp and B_\perp must be continuous across the boundary. What about the normal derivatives of these quantities? To study this we set up an orthogonal n, t coordinate system with its origin at some point on the boundary, wherein the n -axis is along the direction of the normal \hat{n} , at that point, and the t -axis is along the direction of the tangent vector \hat{t} . Then, in terms of these variables the z -component of $\nabla \times \underline{B}$ just outside the guide is $(\nabla \times \underline{B})_z = (\partial B_t / \partial n - \partial B_n / \partial t)_+ = ik B_z = 0$. We can write a similar equation just inside the boundary and hence conclude

$$\left(\frac{\partial B_t}{\partial n} - \frac{\partial B_n}{\partial t} \right)_+ = \left(\frac{\partial B_t}{\partial n} - \frac{\partial B_n}{\partial t} \right)_- \quad (35)$$

Now $\nabla \cdot \underline{B} = 0$, which means that B_n is continuous across the boundary, and, hence, that its tangential derivative $\partial B_n / \partial t$ is also continuous. Then Eq. (35) becomes

$$\left. \frac{\partial B_t}{\partial n} \right|_+ = \left. \frac{\partial B_t}{\partial n} \right|_- \quad (36)$$

In short, the normal derivative of the tangential component is continuous across the boundary. Consider the rectangular components B_x and B_y . If B_x and B_y and their normal derivatives are continuous across the boundary, then the tangential component of B (a linear combination of B_x and B_y) will also have these continuity properties. Arguments similar to the above also apply to E_x and E_y .

Let Φ be either of E_x , E_y , B_x , B_y . Consider Eq. (7) with E_z replaced by Φ :

$$\Phi(\rho) = -(\gamma_1^2 + \gamma_2^2) \int_A \Phi(\rho') g_{\gamma_2}(\rho, \rho') dA' . \quad (37)$$

As we have seen, this guarantees that Eqs. (2) and (3) are satisfied and that Φ and $\partial\Phi/\partial n$ will be continuous across the boundary (Eyges and Nelson¹⁰). If this equation is satisfied, we can take Φ to be either B_x or B_y , or a linear combination of the two of them. This linearly polarized mode will then propagate down the guide of arbitrary cross section with propagation constants and modal characteristics that are governed by Eq. (37) and with an E field that is perpendicular to the B field, as determined by Maxwell's equations. Note that Eq. (37) can be converted to a useful line-integral form by the steps that led from Eq. (16) to Eq. (17). It becomes, for ρ inside the guide,

$$\int_L \left(\Phi - \frac{\partial g_{\gamma_2}}{\partial n'} - \frac{\partial \Phi}{\partial n'} \Big|_- g_{\gamma_2} \right) dL' = 0 . \quad (38)$$

It is worth observing that Eq. (38) can be derived in an alternate way that is related to the so-called Extended Boundary Condition method (EBC) which has recently been exploited for scattering problems (Waterman¹¹). Basic to this method is an integral representation (Huygen's principle) for an amplitude Φ which satisfies $(\nabla^2 - \gamma_2^2)\Phi = 0$ in the exterior region, namely

$$\Phi(\rho) = \int_L \left\{ \Phi + \frac{\partial g_{\gamma_2}}{\partial n'} - \frac{\partial \Phi}{\partial n'} \Big|_+ g_{\gamma_2} \right\} dL' , \quad \rho \text{ outside} . \quad (39)$$

It is well known that if this equation is evaluated in the interior (canonical procedure in the EBC method), it yields zero on the left hand side:

10. Eyges, L. and Nelson, A. E. (1976) Ann. Phys. **100**:37.

11. Waterman, P. C. (1969) J. Acoust. Soc. Am. **45**:1417 and (1971) Phys. Rev. **D3**:825.

$$0 = \int_L \left\{ \Phi_+ \frac{\partial g_{\gamma_2}}{\partial n'} - \frac{\partial \Phi}{\partial n'} \Big|_+ g_{\gamma_2} \right\} dL' \quad , \quad \rho \text{ inside} \quad .$$

But for the present problem we have $\Phi_+ = \Phi_-$ and $\partial \Phi / \partial n|_+ = \partial \Phi / \partial n|_-$ and when these two equations are substituted into the above, the basic Eq. (38) is reproduced.

5. SYMMETRY CONSIDERATIONS

Either of the integral representations (37) or (38) can now be converted to a set of homogeneous linear equations and a corresponding determinantal equation by inserting in them an expansion in the interior solutions $J_s(\gamma_1 \rho) e^{is\phi}$. In fact, it is more convenient to use trigonometric functions, so we shall assume as the general interior expansion for Φ for a guide of arbitrary cross-sectional shape:

$$\Phi(\rho) = \sum_{s=0}^{\infty} J_s(\gamma_1 \rho) \{ C_s \cos(s\phi) + D_s \sin(s\phi) \} \quad . \quad (40)$$

Eq. (40) is in fact too general in that almost all practical guides have symmetry of one kind or another. It is then useful, indeed almost imperative, to sort out in advance the limitations that such symmetry implies for the coefficients in Eq. (40).

In this paper, for example, we shall analyze, among others, guides of rectangular or elliptical cross section. If the axes of such an ellipse or rectangle coincide with the x- and y-axes, then by usual parity arguments of quantum mechanics the amplitude Φ must be either symmetric or antisymmetric about the x-axis. This means that Φ can be expanded in terms of either sines or cosines. Similarly, reflection symmetry about the y-axis can be used to show that both the sine and the cosine expansions split into two other cases, in one of which s runs over even values and in the other over odd values. In short, there are for elliptical or rectangular cross sections (or any guide with similar twofold reflection symmetry) four types of expansions, labelled by R (for rectangle) with superscripts I through IV:

$$R^I: \quad \Phi(\rho) = \sum_{s=0, 2, 4, \dots} C_s J_s(\gamma_1 \rho) \cos(s\phi) \quad (41a)$$

$$R^{II}: \Phi(\underline{\rho}) = \sum_{s=1, 3, 5, \dots} C_s J_s(\gamma_1 \rho) \cos(s\phi) \quad (41b)$$

$$R^{III}: \Phi(\underline{\rho}) = \sum_{s=2, 4, 6, \dots} D_s J_s(\gamma_1 \rho) \sin(s\phi) \quad (41c)$$

$$R^{IV}: \Phi(\underline{\rho}) = \sum_{s=1, 3, 5, \dots} D_s J_s(\gamma_1 \rho) \sin(s\phi) \quad (41d)$$

If, in addition to the twofold symmetry in the perpendicular axes of the rectangle or ellipse, the guide has the symmetry of the square (reflection symmetry with respect to diagonals), the classifications of Eq. (41) are modified in a way that cannot be derived by quite so simple reasoning as the parity arguments above. The results are, however, a straightforward consequence of group theory and of the fact that the symmetry of the square is described by the group C_{4v} , which has four one-dimensional irreducible representations and one two-dimensional one. This leads to the conclusion that there are four expansions, namely, Eqs. (42a-d), which lead to four different (nondegenerate) sets of propagation constants, and two expansions (Eqs. (42e and f)) that yield that same set of propagation constants (degenerate modes). These are

$$R^I \left\{ \begin{aligned} \Phi(\underline{\rho}) &= \sum_{s=0, 4, 8, \dots} C_s J_s(\gamma_1 \rho) \cos(s\phi) \end{aligned} \right. \quad (42a)$$

$$\left\{ \begin{aligned} \Phi(\underline{\rho}) &= \sum_{s=2, 6, 10, \dots} C_s J_s(\gamma_1 \rho) \cos(s\phi) \end{aligned} \right. \quad (42b)$$

$$R^{III} \left\{ \begin{aligned} \Phi(\underline{\rho}) &= \sum_{s=2, 6, 10, \dots} D_s J_s(\gamma_1 \rho) \sin(s\phi) \end{aligned} \right. \quad (42c)$$

$$\left\{ \begin{aligned} \Phi(\underline{\rho}) &= \sum_{s=4, 8, 12, \dots} D_s J_s(\gamma_1 \rho) \sin(s\phi) \end{aligned} \right. \quad (42d)$$

$$R^{II} \phi(\rho) = \sum_{s=1,3,5,\dots} C_s J_s(\gamma_1 \rho) \cos(s\phi) \quad (42e)$$

$$R^{IV} \phi(\rho) = \sum_{s=1,3,5,\dots} D_s J_s(\gamma_1 \rho) \sin(s\phi) \quad (42f)$$

However, in order to relate the modes of the square to their counterparts of the rectangle, we have kept the mode notation introduced in Eq. (41). Thus, in Eq. (42) R^I still refers to "cos, even s" modes and R^{II} to "cos, odd s" modes, etc.

6. EQUATIONS FOR THE WEAKLY GUIDING CASE

Given the expansions of Eq. (41) or (42), we can insert any of them into the integral representations (37) or (38) and use the expansion of the Green function to obtain a set of linear equations and hence a determinantal equation for the modal propagation constants.

One question of strategy is now whether to choose the line integral representation (38) or area integral representation (37). The former choice might appear to be the obvious one since the line integral matrix elements it generates are one-dimensional, and hence ostensibly simpler than the two-dimensional integrals that Eq. (37) would yield. In fact, they are generally simpler and we shall choose to work with Eq. (38), but Eq. (37) should not be set aside completely; it is particularly useful for guides that are not too far from circular. In this case it lends itself to a convenient perturbation analysis (Eyges¹²) in which the integration is broken up into one over a circle (for example, inscribed within the cross section, or of the same area) which generates diagonal matrix elements, and an integral over the remainder area which yields off-diagonal, but small, matrix elements.

For the present work with Eq. (38) we shall need the expansion of the Green function in sines and cosines:

$$g_{\gamma_2}(\rho, \rho') = \frac{-i}{4} \sum_{l=0}^{\infty} \epsilon_l H_l(i\gamma_2 \rho') J_l(\gamma_2 \rho) [\cos l\phi \cos l\phi' + \sin l\phi \sin l\phi'] \quad (43)$$

$\rho < \rho'$

12. Eyges, L. (1978) Appl. Opt. 17:1673.

where ϵ_l , the Neumann factor, is 1 if $l = 0$ and 2 otherwise. The details involved in substituting Eq. (41) or (42) into Eq. (38) are similar to those spelled out in Section 3. The cosine expansions ultimately yield the system of linear homogeneous algebraic equations:

$$\sum_s C_s G_{ls} = 0 \quad (44)$$

whereas, the expansions involving sines eventually produce

$$\sum_s D_s T_{ls} = 0 \quad (45)$$

The indices l and s in the above equations are either both even or both odd and take on the values specified in Eq. (41) or (42). G_{ls} and T_{ls} which are line integrals taken about the perimeter of the guide, are given by:

$$G_{ls} = \int_0^{2\pi} d\phi' [F_{ls}(\rho') \cos l\phi' \cos s\phi' + L_{ls}(\rho', \phi')] \\ \{s \cos l\phi' \sin s\phi' - l \sin l\phi' \cos s\phi'\} \quad (46)$$

$$T_{ls} = \int_0^{2\pi} d\phi' [F_{ls}(\rho') \sin l\phi' \sin s\phi' - L_{ls}(\rho', \phi')] \\ \{s \sin l\phi' \cos s\phi' - l \cos l\phi' \sin s\phi'\} \quad (47)$$

with

$$F_{ls}(\rho') = \epsilon_l \{ \gamma_1 \rho' H_l(i\gamma_2 \rho') J'_s(\gamma_1 \rho') - \gamma_2 \rho' H'_l(i\gamma_2 \rho') J_s(\gamma_1 \rho') \} \quad (48)$$

$$L_{ls}(\rho', \phi') = \epsilon_l H_l(i\gamma_2 \rho') J_s(\gamma_1 \rho') \frac{\partial \phi'}{\partial \phi} / \rho' \quad (49)$$

The related determinantal equations are

$$\det(G_{ls}) = 0 \quad (50)$$

$$\det(T_{ls}) = 0 \quad (51)$$

One can easily recover the familiar dispersion relation for a weakly guiding circular guide of radius a from Eqs. (44) to (49). G becomes diagonal (and identical to T) because $L_{ls} = 0$ and F_{ls} comes outside the integral. Then the condition

$$F_{ll} \propto (\gamma_1 a) H_l'(i\gamma_2 a) J_l'(\gamma_1 a) - (i\gamma_2 a) H_l'(i\gamma_1 a) J_l'(\gamma_2 a) = 0 \quad (52)$$

holds for all l and, when satisfied, gives the modes of the circular guide.

7. COMPUTATIONAL TECHNIQUES

In this section we outline some of the details of our computational techniques. For the work of this paper, Eqs. (48) and (49) are modified in three ways. First, the Bessel function derivatives are eliminated by use of the general recursion relation

$$C_l'(x) = C_{l-1}(x) - \frac{l}{x} C_l(x) \quad (53)$$

Then the Hankel functions are replaced by Modified Bessel functions of the second kind, using

$$H_l(i x) = \frac{2}{\pi} i^{-(l+1)} K_l(x) \quad (54)$$

Finally, the arguments γ_1 and γ_2 are expressed in terms of a normalized propagation constant, P^2 , and a normalized binding constant, β . P^2 , following Goell,² has been normalized so that it varies between 0 and 1 only, while β characterizes the refractive index difference, the smaller guide dimension and operating frequency, hence the extent to which the field exists outside the guide. These quantities are defined to be

$$P^2 = \frac{k_g^2 - k_2^2}{k_1^2 - k_2^2} = \frac{\gamma_2^2}{\gamma_1^2 + \gamma_2^2} \quad (55)$$

$$\beta = \frac{b}{\pi} (k_1^2 - k_2^2)^{1/2} = \frac{b}{\pi} (\gamma_1^2 + \gamma_2^2)^{1/2} = \frac{b k_0}{\pi} (n_1^2 - n_2^2)^{1/2} \quad (56)$$

where b is the semiminor axis of the cross-sectional shape. * One should note that with these definitions specific values of b , k_0 , n_1 , and n_2 are not required. One then obtains

$$\gamma_1 \rho = \pi \beta \sqrt{1 - P^2} \frac{\rho}{b} ; \quad \gamma_2 \rho = \pi P \beta \rho / b . \quad (57)$$

With these modifications, Eqs. (48) and (49) can be rewritten as

$$\begin{aligned} F_{ts}(\rho') = & 2 \epsilon_t \beta \frac{\rho'}{b} i^{-(t+1)} \left\{ K_t \left(\frac{\pi P \beta \rho'}{b} \right) J_{s-1} \left(\frac{\pi \beta \rho'}{b} \sqrt{1 - P^2} \right) \sqrt{1 - P^2} \right. \\ & + P J_s \left(\frac{\pi \beta \rho'}{b} \sqrt{1 - P^2} \right) K_{t-1} \left(\frac{\pi \beta P \rho'}{b} \right) \left. \right\} \\ & + \epsilon_t (t-s) \frac{2}{\pi} i^{-(t+1)} K_t \left(\frac{\pi \beta P \rho'}{b} \right) J_s \left(\frac{\pi \beta \rho'}{b} \sqrt{1 - P^2} \right) \end{aligned} \quad (58)$$

and

$$L_{ts}(\rho', \phi') = \frac{2}{\pi} \epsilon_t i^{-(t+1)} K_t \left(\frac{\pi P \beta \rho'}{b} \right) J_s \left(\frac{\pi \beta \rho'}{b} \sqrt{1 - P^2} \right) \frac{\partial \rho'}{\partial \phi'} / \rho' . \quad (59)$$

To extract numerical results, four things must be done. First, $\rho(\phi)$ must be specified; second, the matrix elements G_{ts} (or T_{ts}) must be computed; third, the roots of the determinantal equation must be found; and finally, for each root, the coefficients C_s (or D_s) are to be found to within a normalizing constant so that the field configuration can be determined from Eq. (41) or (42).

To calculate the line integrals that comprise the matrix elements there are two computational possibilities. One can express the integrands in rectangular coordinates and integrate over dL directly, or one can convert the line integrals to angular ones by writing $dL = (dL/d\phi) d\phi$ and integrate from zero to 2π . The latter procedure is clearly desirable for curved boundaries (for example, ellipses) for which ρ and $\partial\rho/\partial\phi$ are continuous functions of ϕ , but for rectangular cross sections the direct integration seems more straightforward. For the sake of generality in the computer programming, however, we have calculated the matrix elements even for rectangular boundaries by angular integration, using the function

$$\rho(\phi) = b [(\cos^2 \phi / R^2)^N + (\sin^2 \phi)^N]^{-1/2N} \quad (60)$$

* With this definition, β turns out to be one-half of Goell's corresponding quantity, B .

for the perimeter. This gives a figure with a short axis (along $\phi = \pm\pi/2$) of length $2b$ and a long axis (along $\phi = 0, \pi$) equal to $2\tilde{R}b$, where \tilde{R} is the aspect ratio. In general, for arbitrary \tilde{R} , Eq. (60) describes a rectangle if the parameter N is chosen to be infinity (Allard¹³ and Gardner¹⁴) and an ellipse if $N = 1$. Shapes with $1 < N < \infty$ are called "superellipses" (Gardner¹⁴) and can be regarded as a continuous deformation of an ellipse into a rectangle as N increases. Shapes with $0.5 < N < 1$ are called "subellipses" (Gardner¹⁴) and can be regarded as a continuous deformation of an ellipse into a parallelogram. $N = 0.5$ gives a parallelogram, and if $0 < N < 0.5$ one obtains figures with four cusps, tending toward crossed straight lines as $N \rightarrow 0$. Whenever $\tilde{R} = 1$ in the above analysis, the rectangle and the ellipse become the square and the circle, respectively.

In Figure 2 we show the first quadrant of some of the shapes obtainable for various N with $\tilde{R} = 1$. Regardless of the values of N or \tilde{R} in Eq. (60), reflection symmetry about the x - and y -axes produces a closed figure throughout the four quadrants. Thus, use of Eq. (60) assures continuity of $d\rho/d\phi$ over the entire range of ϕ , thereby eliminating the need of subdividing ϕ into several intervals whose boundaries depend on \tilde{R} .

The fractional error one makes in taking Eq. (60) as an approximation to a rectangle is, for a given value of N , independent of \tilde{R} . The error in $\rho(\phi)$ is worst at the corners but becomes small very rapidly for values of ϕ away from the corners. We used $N = 30$, which gives a fractional error of 0.012 at the corners, 0.002 one degree away, and 0.00025 two degrees away. For $N = 10$ the values at the same three angular positions are 0.034, 0.020, and 0.011 respectively.

Because of symmetry, the integrals (46) and (47) need to be done only over the interval $(0, \pi/2)$. With the transformation $z = -\cos 2\phi$, they become susceptible to Chebyshev integration (Hildebrand¹⁵) which takes equally spaced points in the range $(-1, 1)$ with equal weights. Generally, 50 points were sufficient to obtain the required accuracy, although checks were made with many more.

In order to satisfy Eq. (50) or (51), the determinants were truncated and then evaluated at equally spaced values of P^2 . The roots were located approximately from the table of these results, and a half-interval search (Hornbeck¹⁶) was used to pin down the values of P^2 to four significant figures. The number of terms to retain was determined empirically, with two terms being sufficient in many cases. For a given mode of a given guide, the number of terms needed for a certain

13. Allard, J. (1964) *Math. Mag.* 37:210.

14. Gardner, M. (1965) *Sci. Am.* 213:222.

15. Hildebrand, F.B. (1956) *Introduction to Numerical Analysis*, McGraw Hill, N.Y., p 330.

16. Hornbeck, R.W. (1975) *Numerical Methods*, Quantum Publishers, N.Y., p 65.

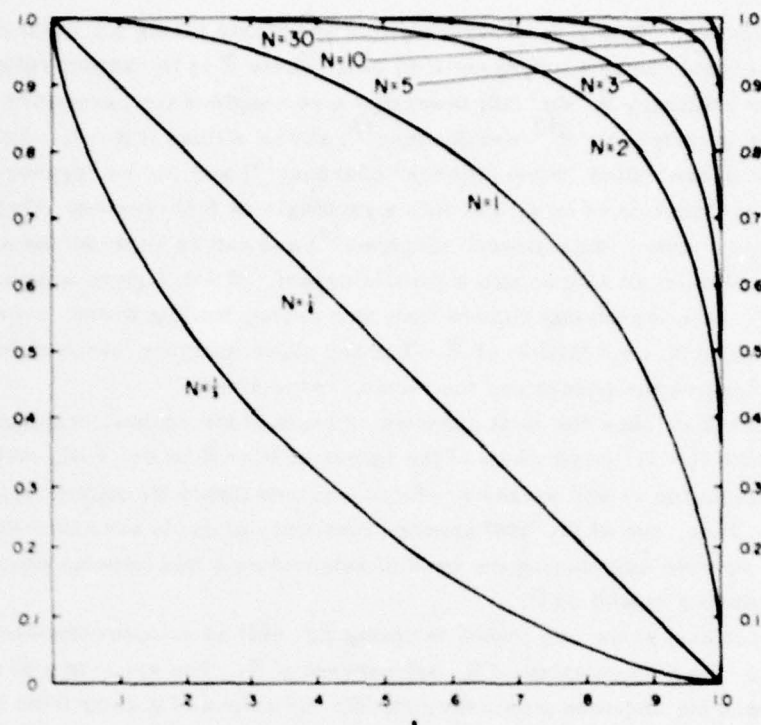


Figure 2. Plot of the Function $\rho(\phi)$ Given in Equation (60) for $0 \leq \phi \leq \pi/2$ Only, $\tilde{R} = 1$, and Various Values of N

absolute accuracy in P^2 does not depend on β . However, in general, different modes require different numbers of terms to give results with the same accuracy. The computations were carried out on a CDC-6600 computer. The time required is nearly proportional to the square of the dimension of the determinant, for a given number of roots and accuracy. Thus, a three-term truncation procedure might use 30 sec to locate three roots to within 0.0001. Using four or more terms, it is usually possible to search a limited region near a root and thus save time.

8. RESULTS AND COMPARISON WITH OTHER WORK

We have investigated the properties of weakly guiding waveguides having all of the various cross sections described in Section 7 and aspect ratios ranging between 1 and 10. In this section we present some of our results, to demonstrate the utility of the method and make comparisons with previously published work for the more common shapes.

8.1 Rectangular Cross Sections

For the rectangular waveguides having aspect ratios $1 \leq \tilde{R} \leq 2$ we have located more than two dozen modes in the range $0 < \beta < 4$. The curves for the propagation constants (P^2 versus β) corresponding to approximately the first dozen modes for each aspect ratio are plotted in Figures 3, 4, 5, and 6 for β values up to 2.5. Each of these curves corresponds to one of four types of field function when $\tilde{R} > 1$ (see Eq. (41)) or one of six types when $\tilde{R} = 1$ (see Eq. (42)). These field functions are designated R^I through R^{IV} . The mode corresponding to the n -th root of the X -th type of determinant (see Eq. (50) or (51)) is designated R_n^X . (Thus, the first (nongutoff) mode is labelled R_1^I because it involves a cosine expansion with even indices.) The ordering within a family is governed by the value of β at which cutoff occurs; $n = 1$ designating the mode which cuts off at the smallest β . Since for $\tilde{R} > 1$ certain modes "cross over" (for example, see R_3^I and R_4^I in Figure 6), this choice must be kept in mind when considering modes at values of β above the crossover point (for example, see the values of β for these same two modes in Table 4).

As was noted in Section 5, the special symmetry of the square causes the even expansions to split into two series each. Thus, consider the two cosine expansions of Eqs. (42a and b): The first mode determined using Eq. (42a) is the first member of the R^I family (that is, R_1^I) and its field expansion is given as $C_0 J_0 + C_4 J_4 \cos 4\phi + \dots$. Whereas, the first mode determined using Eq. (42b) turns out to be the third member of the same family (hence, R_3^I) whose field expansion has the form $C_2 J_2 \cos 2\phi + C_6 J_6 \cos 6\phi + \dots$. However, for the rectangular cross sections ($\tilde{R} > 1$), the field expansions for all even cosine modes take the form $C_0 J_0 + C_2 J_2 \cos 2\phi + C_4 J_4 \cos 4\phi + \dots$.

A crucial question underlying our approach is: How many terms must be kept in the determinantal Eqs. (50) and (51) in order for the roots to converge to definite values? We now address this question.

The convergence of the R_1^I expansion is rapid for both the square and rectangular guides. For the square guide, Table 1 gives the values of P^2 obtained for this mode after truncation of Eq. (50) at 1, 2, or 3 terms for selected values of β . Clearly, the two-term truncation is only a small improvement, in terms of locating the roots, on the single-term result, which is obtained by setting $G_{00} = 0$ in Eq. (50). Moreover, the extra work involved in taking three terms leads to no gain whatsoever. In view of this, it is reassuring that the ratios of the second term of the field expansion to the first ($C_4 J_4 / C_0 J_0$), and the third to the first ($C_8 J_8 / C_0 J_0$) show that the J_0 term is dominant for this mode. The term ratios listed in the 5th and 6th columns of Table 1 were evaluated on the perimeter at the middle of one side (that is, $\rho = b$, $\phi = 0$). Since J_4 and J_8 become smaller as ρ

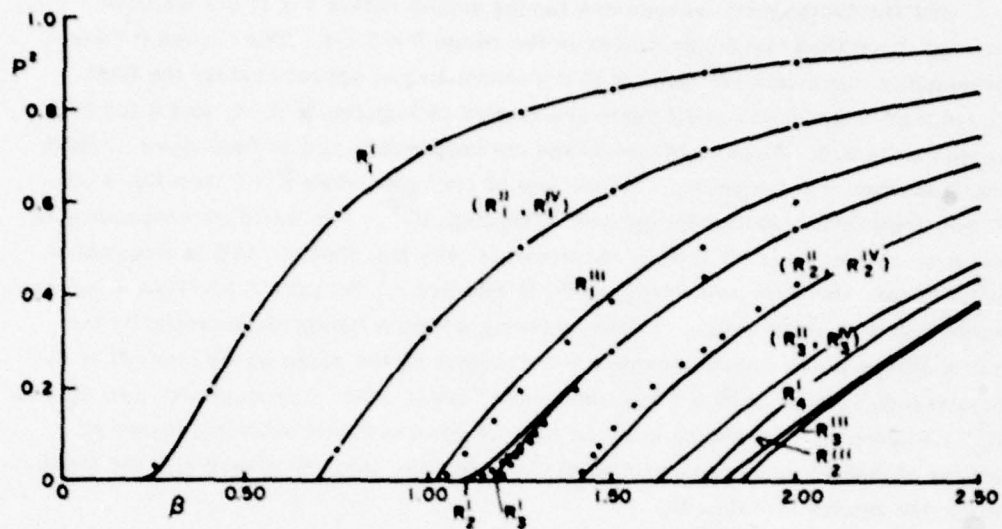


Figure 3. Modes of the Weakly Guiding Square Guide. Dots were taken from Figure 16 of Goell²

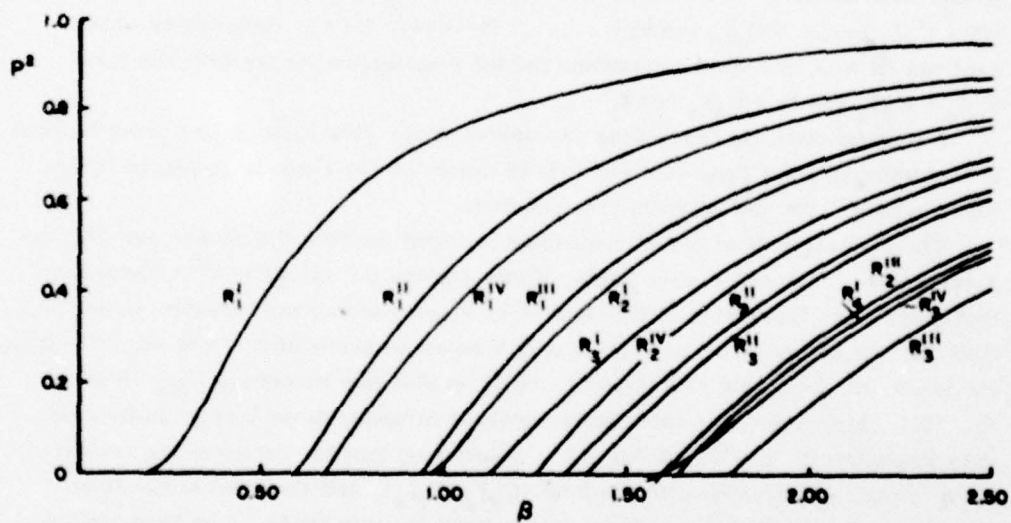


Figure 4. Modes of the Weakly Guiding Rectangular Guide with $\tilde{R} = 1.2$

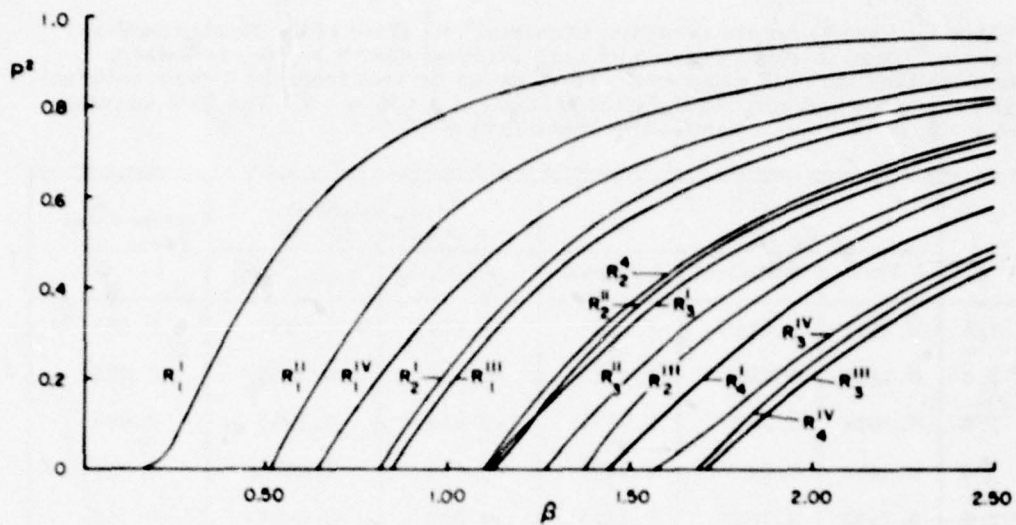


Figure 5. Modes of the Weakly Guiding Rectangular Guide with $\tilde{R} = 1.5$

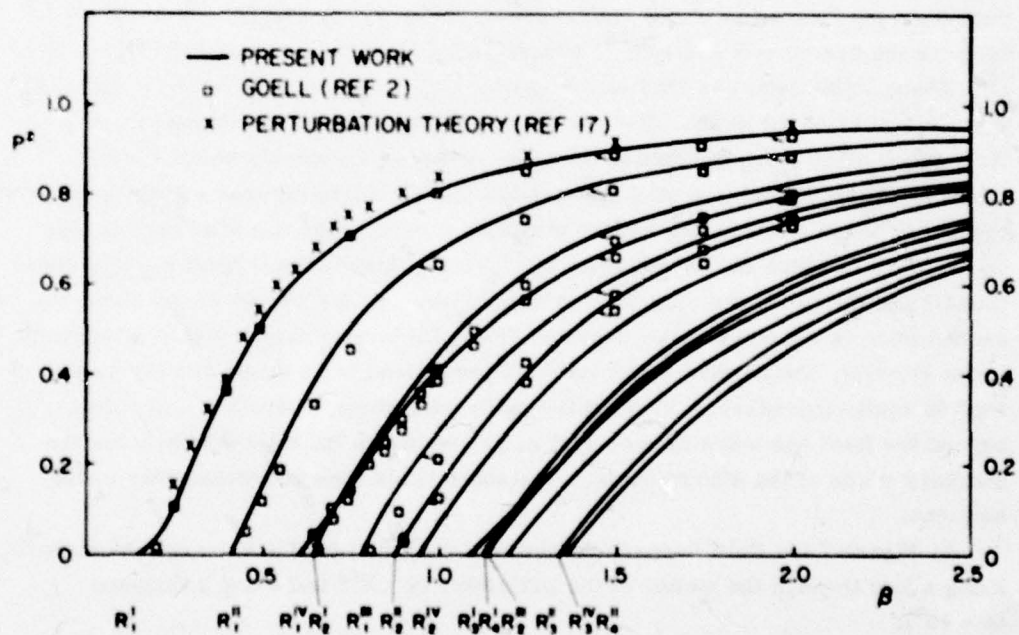


Figure 6. Modes of the Weakly Guiding Rectangular Guide with $\tilde{R} = 2$. Square points were taken from Figure 17 of Goell.² X's represent results of a perturbation calculation for the R_1^I mode

Table 1. Results for the Dominant (Noncutoff) R_1^1 Mode of the Weakly Guiding Square Guide. Listed values of P^2 were obtained after a 1-, 2-, or 3-term truncation of the field expansion. Term ratios derived from the 3-term solution give $C_4 J_4 \cos 4\phi / C_0 J_0$ and $C_8 J_8 \cos 8\phi / C_0 J_0$ at $\rho = b$, $\phi = 0$. The field intensity at $\rho = b$, $\phi = 0$ is also given. The intensity at $\rho = 0$ is 1

β	P^2			Term Ratios at Perimeter ($\phi = 0$)		Intensity at Perimeter ($\phi = 0$)
	1 Term	2 Terms	3 Terms	$C_4 J_4 / C_0 J_0$	$C_8 J_8 / C_0 J_0$	
3.0	0.9511	0.9546	0.9546	-0.314	0.0006	0.023
2.5	0.9329	0.9371	0.9372	-0.266	0.0009	0.032
2.0	0.9023	0.9072	0.9072	-0.213	0.0005	0.046
1.5	0.8442	0.8497	0.8497	-0.153	0.0005	0.076
1.0	0.7122	0.7175	0.7175	-0.089	0.0004	0.143
0.5	0.3263	0.3290	0.3291	-0.029	0.0003	0.371

decreases, the term ratios are generally greatest at the perimeter and as such constitute the "worst case" for convergence. (For $\beta = 3$ at $(\rho, \phi) = (0.5b, 0)$ the term ratios are -0.007 and $<10^{-5}$, respectively. The intensity is 0.576.)

Table 1 also lists the field intensity at $\rho = b$, $\phi = 0$, normalized to a value of 1 at the center of the guide. For the more tightly bound cases, (higher β), the field drops off to a few percent at the edge, whereas for weakly bound cases (smaller β) the intensity is still appreciable there, indicating that a greater fraction of the beam is extending beyond the guiding core. One can also see that for those cases in which the second term ($C_4 J_4 / C_0 J_0$) makes the largest percent contribution to the field, the total field is small; whereas for weakly bound cases the second term is a much smaller fraction of a considerably larger field. (Similarly, in the interior, the percent contribution of the second term drops quickly as the field intensity increases.) Viewing the guide as a whole, therefore, all terms beyond the first one make unimportant contributions to the total intensity for the dominant mode of the square guide. The same holds true for rectangular cross sections.

In Figure 7 the field intensity is plotted as a function of ρ/b for this mode both along a line through the center of the perimeter ($\phi = 0^\circ$) and along a diagonal ($\phi = 45^\circ$).

We also obtain good convergence of the field expansions for the remaining (cutoff) modes. Table 2 compares the 1-, 2-, 3-, and 4-term truncation results of Eq. (50) or (51) for the first several models of the square. Comparing the

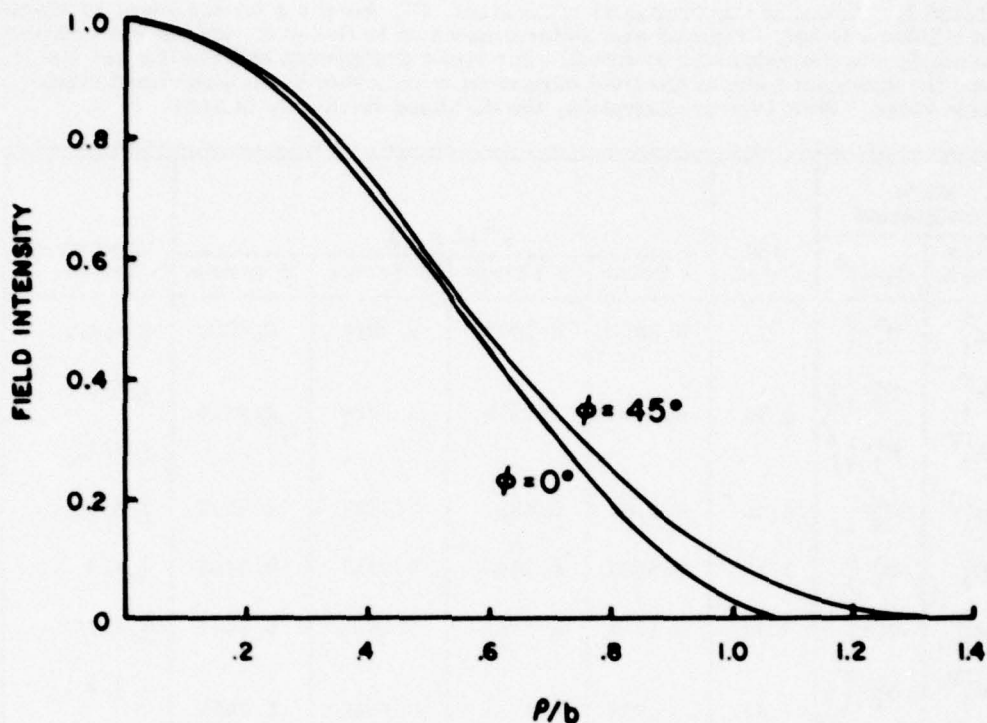


Figure 7. Field Intensity as a Function of p/b for the R_1^I Mode of a Square Guide with $\beta = 3$. The two values of ϕ chosen represent the extremes of the intensity distribution

2- and 4-term truncations, we see that only two terms are required for an accuracy of 0.01 in P^2 for 7 of the first 13 modes of the square. As for the remaining modes, three terms are sufficient to bring the accuracy to within 0.01, except for the degenerate $R_2^{II}-R_2^{IV}$ mode, which is accurate to within 0.02.

Table 2, which also lists the mode designations, specifies in its last column which term is dominant in the field expansion. This is indicated by the underlined value. Thus, we see that for most of the modes the first term does dominate, and it is this term used alone in Eq. (50) or (51) which produces the 1-term truncation result in Table 2. For example, $G_{22} = 0$ was used for the R_3^I mode, $T_{22} = 0$ for the R_1^{III} , $T_{44} = 0$ for the R_3^{III} and either G_{11} or $T_{11} = 0$ for the degenerate $R_1^{II}-R_1^{IV}$ mode. The observation stated above concerning the R_1^I mode is generally applicable to these other modes. That is, for many modes the higher terms in the expansion are comparable in magnitude to the first term only where the field intensity is small; otherwise, they are negligible.

Table 2. Values of the Propagation Constant, P^2 , for $\beta = 2$ for the First 13 Modes of a Square Guide, Obtained with Determinants up to Order 4. Modes are ordered according to the value of β at cutoff. Our mode designation and Goell's are listed, and the dominant term in the field expansion is indicated by an underlined expansion index. With 1-term truncation, the dominant term only is used

Mode Designation		β at Cutoff	P^2 at $\beta = 2$				Expansion Indices
This Work	Goell ²		1 Term	2 Terms	3 Terms	4 Terms	
R_1^I	$E_{11}^{x,y}$	0	0.9023	0.9072	0.9072	0.9072	<u>0</u> , 4, 8, ...
R_1^{II}	$E_{21}^{x,y}$	0.70	0.7546	0.7614	0.7688	0.7695	<u>1</u> , 3, 5, ...
R_1^{IV}							
R_1^{III}	$E_{22}^{x,y}$	1.04	0.6107	0.6321	0.6323	0.6323	<u>2</u> , 6, 10, ...
R_2^I	$E_{31}^{x,y}$	1.10	0.5037	0.5410	0.5457	0.5458	<u>0</u> , 4, 8, ...
R_3^I	$E_{13}^{x,y}$	1.17	0.5390	0.5446	0.5446	0.5446	<u>2</u> , 6, 10, ...
R_2^{IV}	$E_{23}^{x,y}$	1.41	0.3383	0.3754	0.3850	0.4071	<u>1</u> , <u>3</u> , 5, ...
R_2^{II}							
R_3^{II}	$E_{32}^{x,y}$	1.62	0.2300	0.2230	0.2461	0.2447	<u>1</u> , 3, 5, ...
R_3^{IV}							
R_4^I		1.74	0.0784	0.1508	0.1892	0.1902	<u>0</u> , <u>4</u> , 8, ...
R_2^{III}		1.81	0.0591	0.1118	0.1240	0.1243	<u>2</u> , 6, 10, ...
R_3^{III}		1.87	0.0914	0.1091	0.1089	0.1089	<u>4</u> , 8, 12, ...

However, there are some modes for which the second term in the field expansion is the most important one. For example, the field intensity of the R_4^I mode of the square guide is plotted in Figure 8. It shows peaks at two different radial distances from the center. In the peak near the origin, the C_0J_0 term turns out to be the dominant one, but in the second peak the first term ratio has values ranging up to 20 and is consistently greater than 1, showing that the $C_4J_4 \cos 4\phi$ term is the most important one there. For this mode setting only $G_{44} = 0$ produces the 1-term truncation result shown in Table 2. Another example in which the second

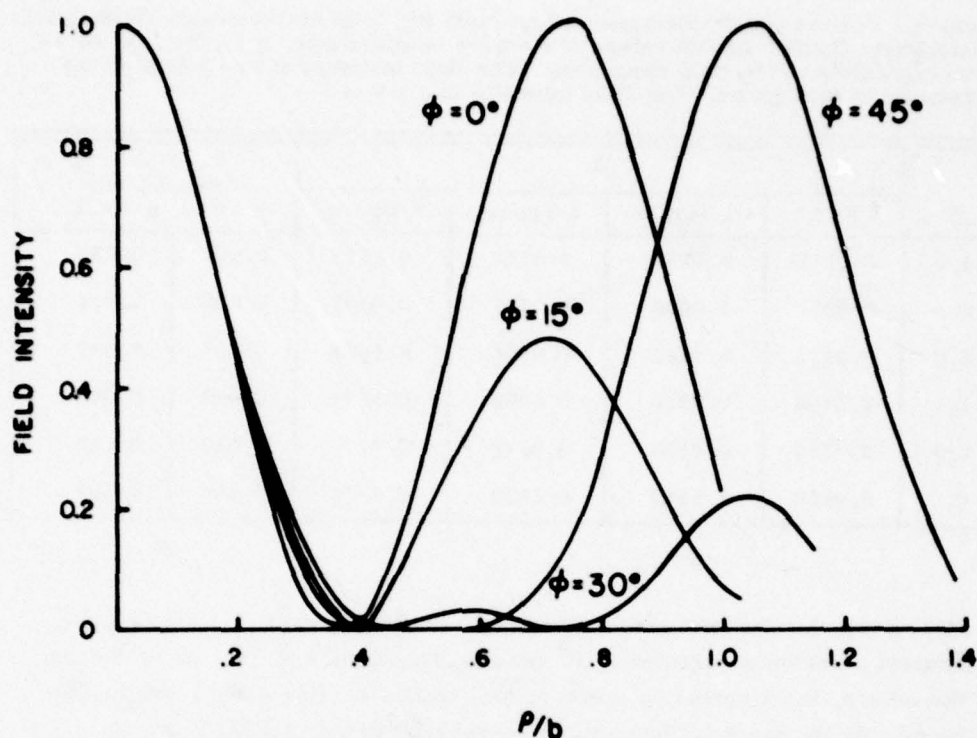


Figure 8. Field Intensity as a Function of ρ/b for the R_4^I Mode of the Square Guide with $\beta = 3$ and Various Values of ϕ . When $\rho > 0.4b$ the second term ($C_4 J_4 \cos 4\phi$) dominates the field expansion. (See text)

term predominates is the degenerate $R_2^{IV}-R_2^{II}$ mode. Here, the 1-term truncation result was obtained by setting either G_{33} or $T_{33} = 0$. In such cases as these, it is obvious from a perusal of the Table 2 results that a 1-term truncation is inadequate for proper convergence and that at least three terms in the expansion are necessary.

The mode R_2^{III} is an example in which even though the first term is dominant, the other terms are still making a significant contribution. From Table 2 one can see that here, also, three terms are required in the expansion.

Tables 3 and 4 give the same type of information for the $\tilde{R} = 2$ rectangle as Tables 1 and 2 did for the square. One would expect the convergence at a given order of truncation to become increasingly worse for higher and higher modes. This is borne out in Table 4. Here are shown the effects on P^2 of truncating up to seventh order for the first 13 modes of the $\tilde{R} = 2$ rectangular guide at a fixed value of β . These results demonstrate that either a 2- or 3-term truncation is sufficient for an accuracy of 0.01 or less in P^2 for 7 of 13 modes of this rectangle.

Table 3. Results for the Dominant (Noncutoff) R_1^I Mode of the Weakly Guiding 2:1 Rectangular Guide. Listed values of P^2 were obtained after a 1-, 2-, 3-, or 4-term truncation of the field expansion. The field intensity at two points on the perimeter is also given. The field intensity at $\rho = 0$ is 1

β	P^2				Intensity at	
	1 Term	2 Terms	3 Terms	4 Terms	$\phi = 0$	$\phi = \pi/2$
3.0	0.9512	0.9732	0.9726	0.9711	0.007	0.023
2.5	0.9333	0.9628	0.9607	0.9597	0.009	0.031
2.0	0.9035	0.9444	0.9406	0.9402	0.013	0.047
1.5	0.8488	0.9074	0.9022	0.9021	0.023	0.075
1.0	0.7354	0.8170	0.8116	0.8118	0.047	0.142
0.5	0.4456	0.5149	0.5122	0.5124	0.155	0.355

Furthermore, for the first mode of each family (that is, R_1^X), the single-term truncation provides accuracies in P^2 ranging from 0.04 to 0.14. As in the case of the square, the 1-term truncation results shown in Table 4 were obtained by utilizing only the dominant term in the appropriate determinantal Eq. (50) or (51).

8.2 Elliptical Cross Sections

The same calculations which were performed for rectangular guides were repeated using circular ($\tilde{R} = 1$) and elliptical ($\tilde{R} > 1$) cross sections. Although the modes for the generalized ellipse are described mathematically by the same four forms listed in Eq. (41), they are labelled E_n^I through E_n^{IV} in order to identify them as pertaining to the ellipse.

The propagation constants of the circular guide, which are the same (that is, degenerate) for the sine and cosine modes, derive from single-term truncation. They are shown over the range $0 \leq \beta \leq 2.5$ in Figure 9. As \tilde{R} increases from 1 to 2, the sine and cosine modes split and shift. The results for ellipses with $\tilde{R} = 1.2$, 1.5 and 2 are depicted in Figures 10, 11, and 12, respectively. These modes are qualitatively very similar to those of their rectangular counterparts shown in Figures 4, 5, and 6. In fact, if one makes the correspondence $E_n^X \sim R_n^X$, then the order in which the first dozen modes of the elliptical guides reach cutoff is nearly the same as the order for the rectangular guides. Moreover, the actual values of β at cutoff are similar for the two shapes for all \tilde{R} . Table 5 gives the actual values of β at cutoff for ellipses with $1 \leq \tilde{R} \leq 2$ and also, for comparison, for the

Table 4. Results for the First 13 Modes of the 2:1 Rectangular Guide, Ordered According to the Value of β at Cutoff. Values of p^2 were obtained for $\beta = 2$, from the roots of determinants 1×1 to 7×7 in dimension. Our designation and Goell's are listed. The dominant term in the field expansion is indicated by an underlined expansion index. With 1-term truncation, the dominant term only is used. For certain modes 2-term truncation failed to locate the roots at certain values of β .

Mode Designation		β at Cutoff	p^2 at $\beta = 2$							Expansion Indices
This Work	Goell ²		1 Term	2 Terms	3 Terms	4 Terms	5 Terms	6 Terms	7 Terms	
I R ₁	$E_{1,1}^{x,y}$	0	0.9035	0.9444	0.9406	0.9402	0.9402	0.9402	0.9402	<u>0</u> , 2, 4, ...
II R ₁	$E_{2,1}^{x,y}$	0.42	0.7974	0.9141	0.9001	0.9001	0.9001	0.9001	0.9001	<u>1</u> , 3, 5, ...
IV R ₁	$E_{1,2}^{x,y}$	0.60	0.7516	0.7959	0.8044	0.8025	0.8025	0.8023	0.8023	<u>1</u> , 3, 5, ...
I R ₂	$E_{3,1}^{x,y}$	0.64	0.5380	---	0.8482	0.8338	0.8335	0.8334	0.8334	0, <u>2</u> , 4, ...
III R ₁	$E_{2,2}^{x,y}$	0.77	0.6206	0.7531	0.7684	0.7620	0.7622	0.7622	0.7622	<u>2</u> , 4, 6, ...
II R ₂	$E_{4,1}^{x,y}$	0.87	0.3318	---	0.7470	0.7430	0.7405	0.7405	0.7405	<u>1</u> , 3, 5, ...
IV R ₂		0.95	0.2935	0.4273	0.6934	0.7006	0.6954	0.6957	0.6957	<u>1</u> , 3, 5, ...
I R ₃		1.08	0.0786	---	0.4935	0.5752	0.5785	0.5777	0.5776	0, <u>2</u> , 4, ...
I R ₄		1.12	0.3068	---	0.5723	0.6186	0.6281	0.6216	0.6219	<u>0</u> , 2, 4, ...
III R ₂		1.14	0.0849	---	0.6101	0.6035	0.6036	0.6031	0.6030	<u>2</u> , 4, 6, ...
II R ₃		1.18	0.3823	---	0.5080	0.5353	0.5409	0.5375	0.5377	<u>1</u> , 3, 5, ...
IV R ₃		1.33	0.2174	0.2745	0.2681	0.4942	0.4619	0.4868	0.4848	<u>1</u> , 3, 5, ...
II R ₄		1.35	---	0.2667	0.4115	0.4697	0.4876	0.4783	0.4786	

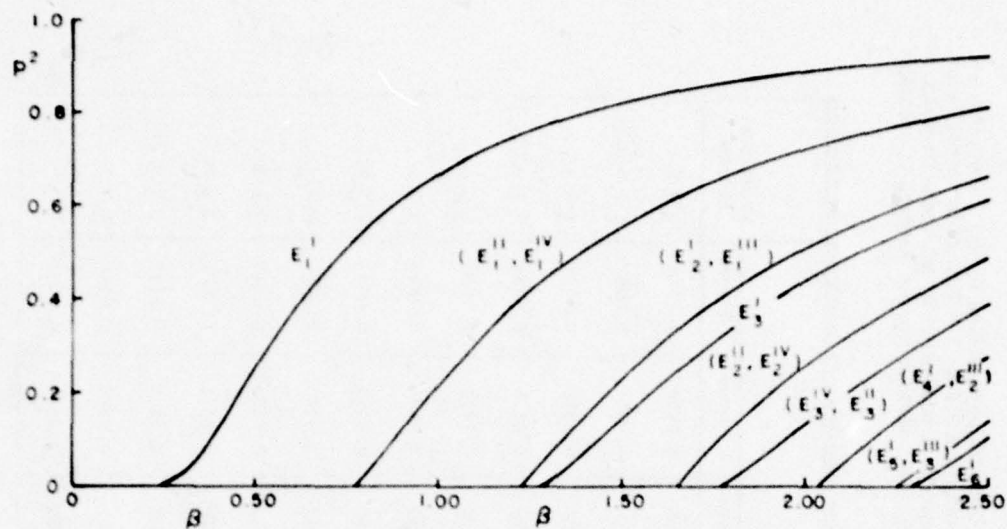


Figure 9. Modes of the Weakly Guiding Circular Guide

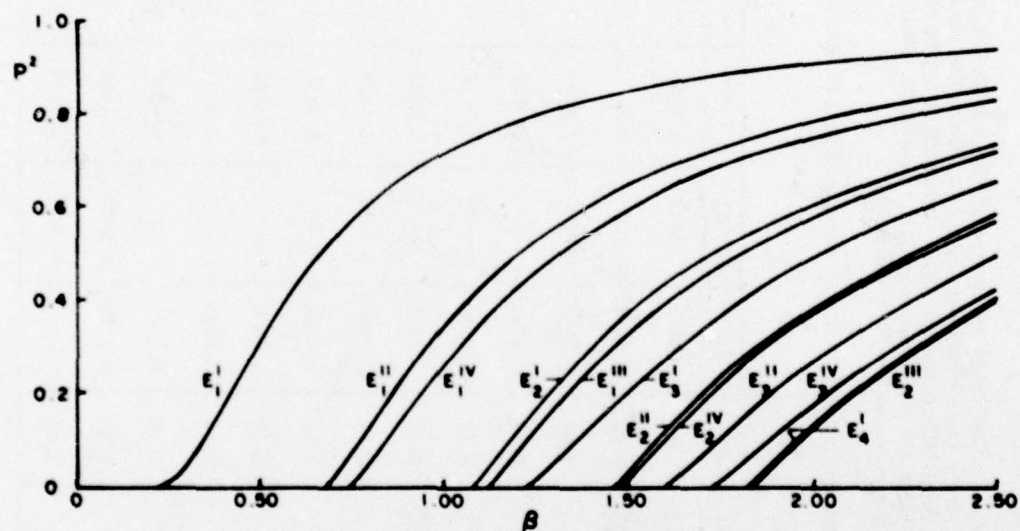


Figure 10. Modes of the Weakly Guiding Elliptical Guide with $\bar{R} = 1.2$

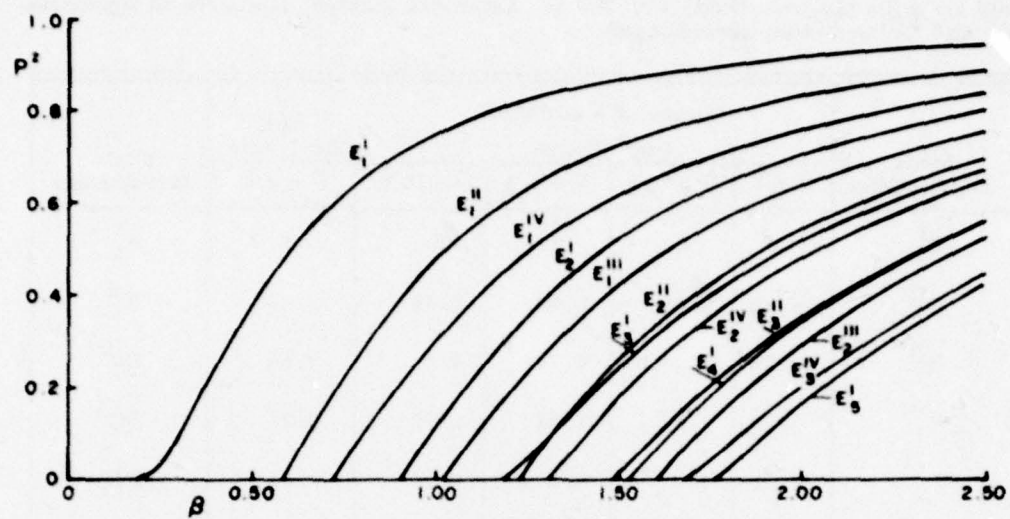


Figure 11. Modes of the Weakly Guiding Elliptical Guide with $\tilde{R} = 1.5$

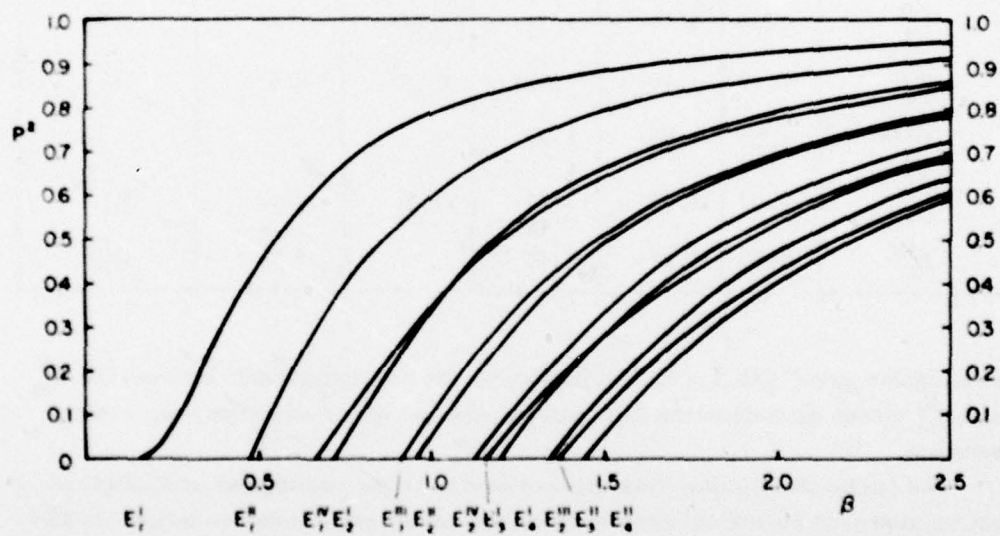


Figure 12. Modes of the Weakly Guiding Elliptical Guide with $\tilde{R} = 2$

Table 5. Values of β at Cutoff for Elliptical Guides with Different Aspect Ratios and for a Rectangular Guide with $\tilde{R} = 2$. Asterisks indicate where the designations E_2^{II} and E_3^{II} should be interchanged

Mode Designation	Values of β at Cutoff					Mode Designation
	For Ellipse				For Rectangle	
	$\tilde{R} = 1$	$\tilde{R} = 1.2$	$\tilde{R} = 1.5$	$\tilde{R} = 2.0$	$\tilde{R} = 2.0$	
E_1^{I}	0	0	0	0	0	R_1^{I}
E_1^{II}	0.78	0.68	0.58	0.48	0.42	R_1^{II}
E_1^{IV}	0.78	0.74	0.72	0.67	0.60	R_1^{IV}
E_1^{III}	1.23	1.12	1.01	0.92	0.77	R_1^{III}
E_2^{I}	1.23	1.07	0.89	0.72	0.64	R_2^{I}
E_3^{I}	1.28	1.22	1.18	1.15	1.08	R_3^{I}
E_2^{IV}	1.65	1.48	1.30	1.13	0.95	R_2^{IV}
E_2^{II}	1.65	1.59*	1.48*	1.37*	1.18	R_3^{II}
E_3^{II}	1.77	1.46*	1.22*	0.96*	0.87	R_2^{II}
E_3^{IV}	1.77	1.72	1.68			
E_4^{I}	2.03	1.82	1.52	1.20	1.12	R_4^{I}
E_2^{III}	2.03	1.83	1.60	1.35	1.14	R_2^{III}

rectangular guide with $\tilde{R} = 2$. Furthermore, the correspondence between the E_m^{X} and R_m^{X} modes extends to the field configurations, which comprise very similar patterns.

The qualitative similarities between modes of the rectangular and elliptical guides approach numerical agreement as the aspect ratio becomes large. In fact, for $R = 10$ the first few modes of either shape guide are virtually indistinguishable for $\beta > 1.5$. In general, the propagation constants for either differ by more than 0.03 only very close to cutoff.

8.3 Other Shapes

We have used our technique to study the propagation modes of guides of certain other shapes obtainable from Eq. (60), mostly with $\tilde{R} = 1$. Among these were superellipses with $N = 2$ and $N = 5$, and a cusped shape deriving from $N = 0.3$. See Figures 13 through 15.

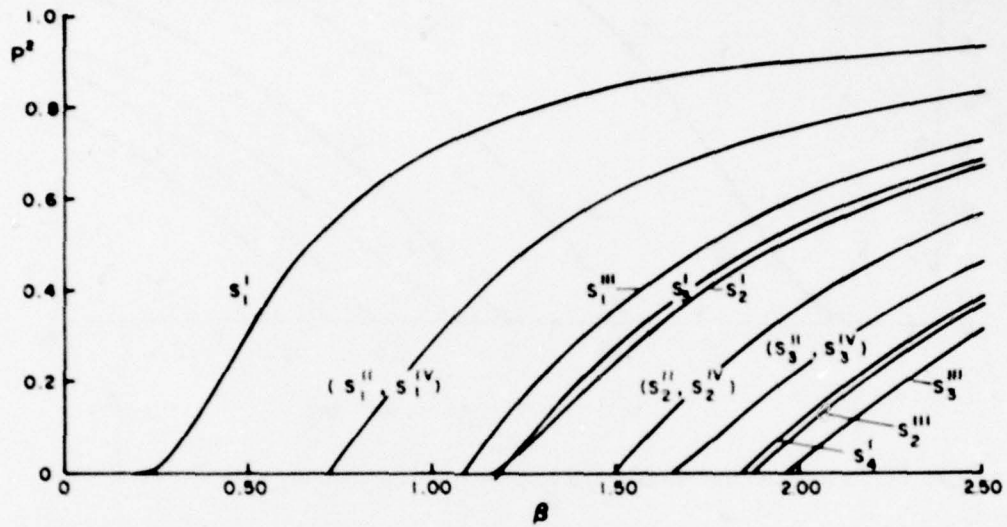


Figure 13. Modes of the Weakly Guiding Superelliptical Guide with $\tilde{R} = 1$, $N = 2$

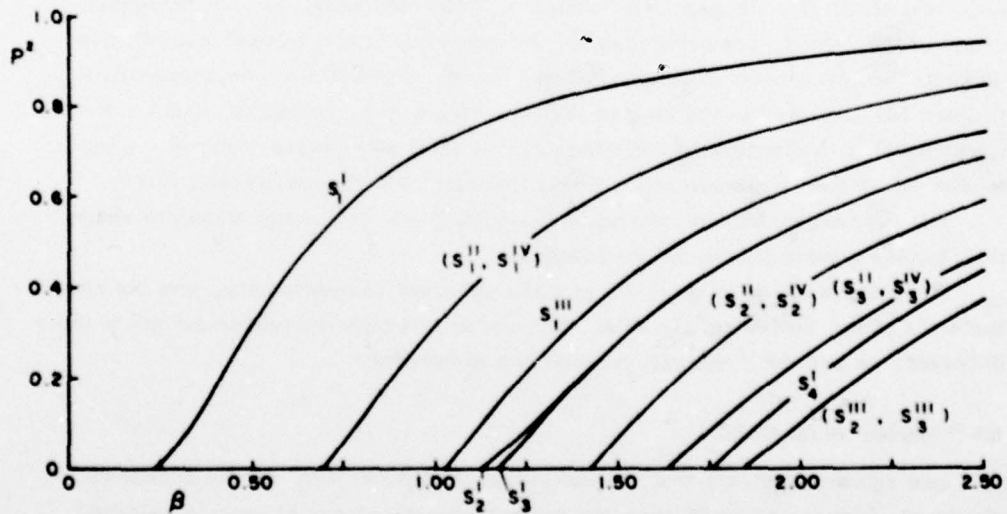


Figure 14. Modes of the Weakly Guiding Superelliptical Guide with $\tilde{R} = 1$, $N = 5$

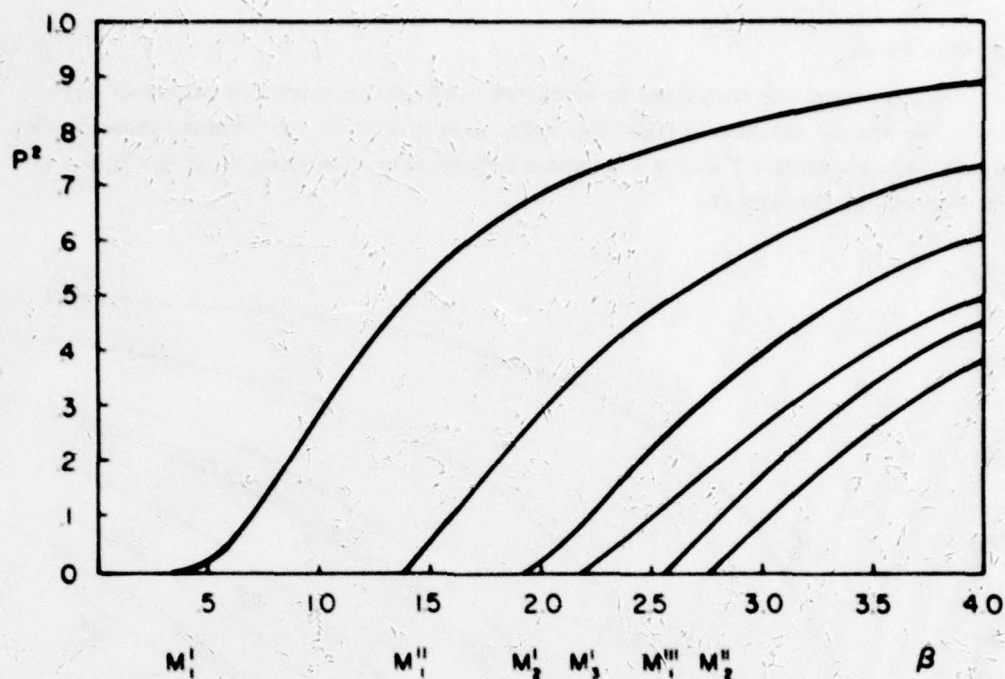


Figure 15. Modes of the Weakly Guiding Cusp-Shaped Guide with $\tilde{R} = 1$, $N = 0.3$

There are many similarities between the elliptical and rectangular guides, so it is no surprise that all the measurable characteristics of the intermediate super-elliptical shape (the propagation constants, field configurations, cutoff values, order of the modes, dependence on \tilde{R} , convergence of the series) fall between those of the two former shapes. In fact, for $N = 2$ and $\tilde{R} = 1$, the superellipse (Figure 13) is closer to the square than the circle in all respects, and for $N = 5$ (Figure 14) it is practically indistinguishable from the square. For $\tilde{R} = 1$ the modes all shift in a smooth and orderly manner as N changes from 1 to 30.

The convergence of the series is marginally better for the elliptical shape than for the superellipses and rectangles.

The cusped shape (Figure 15) is quite different in appearance, and the characteristics of the modes reflect this. The order in which the modes cut off is quite different, as are the propagation constants themselves.

8.4 "Evolution" of the Modes

One can demonstrate that the individual modes "evolve" as the aspect ratio changes. Figures 16 to 20 show the propagation constants of certain selected

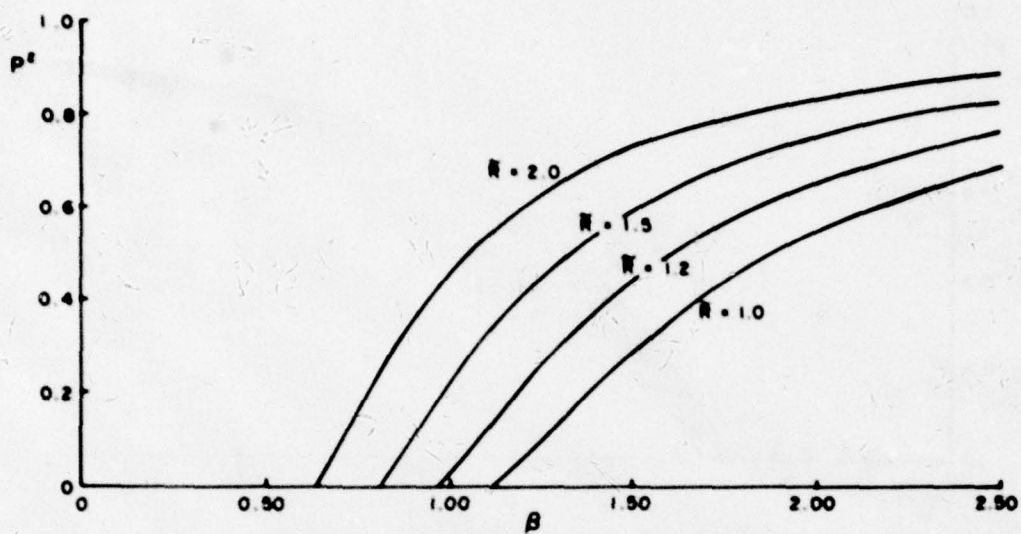


Figure 16. The R_2^I Mode of the Weakly Guiding Rectangular Guide as \tilde{R} Changes from 1 to 2

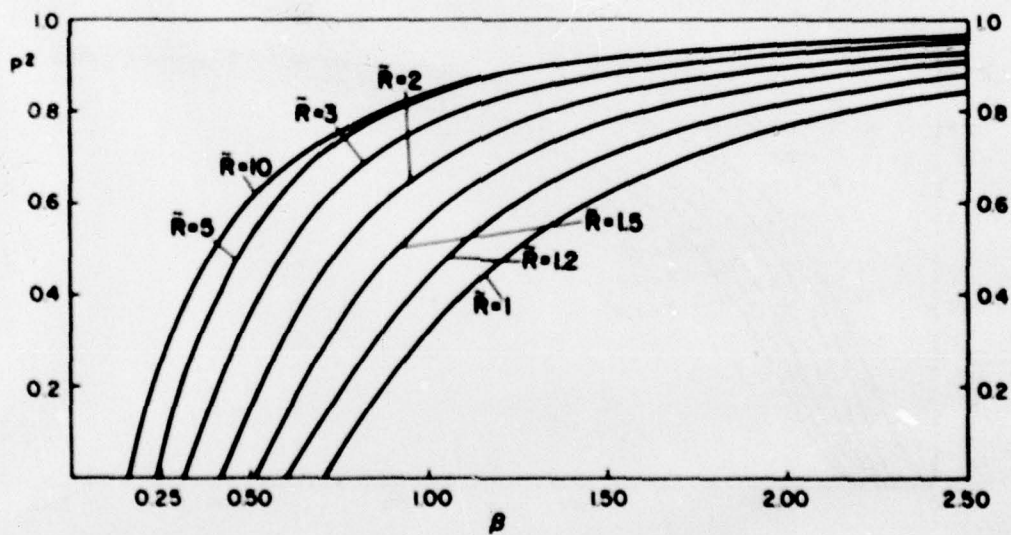


Figure 17. The R_1^{II} Mode of the Weakly Guiding Rectangular Guide as \tilde{R} Changes from 1 to 10

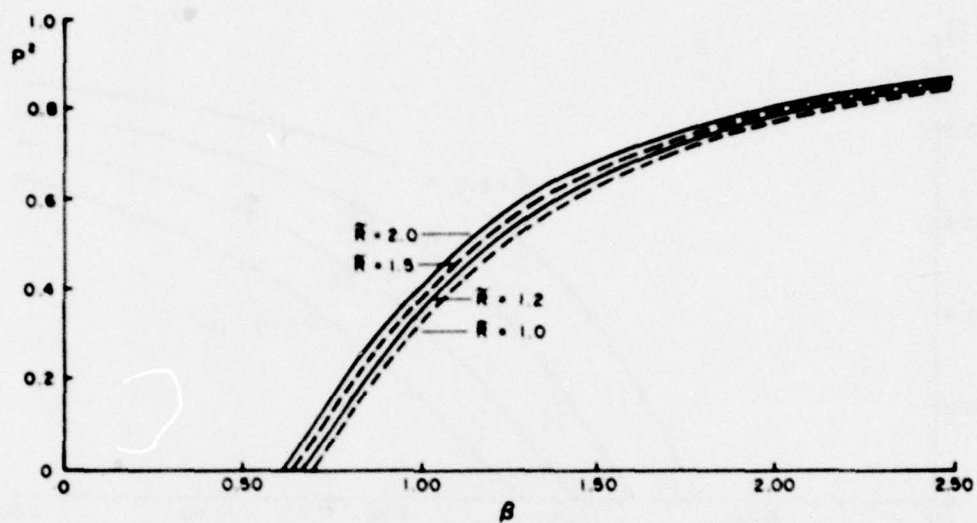


Figure 18. The R_1^{IV} Mode of the Weakly Guiding Rectangular Guide as \tilde{R} Changes from 1 to 2

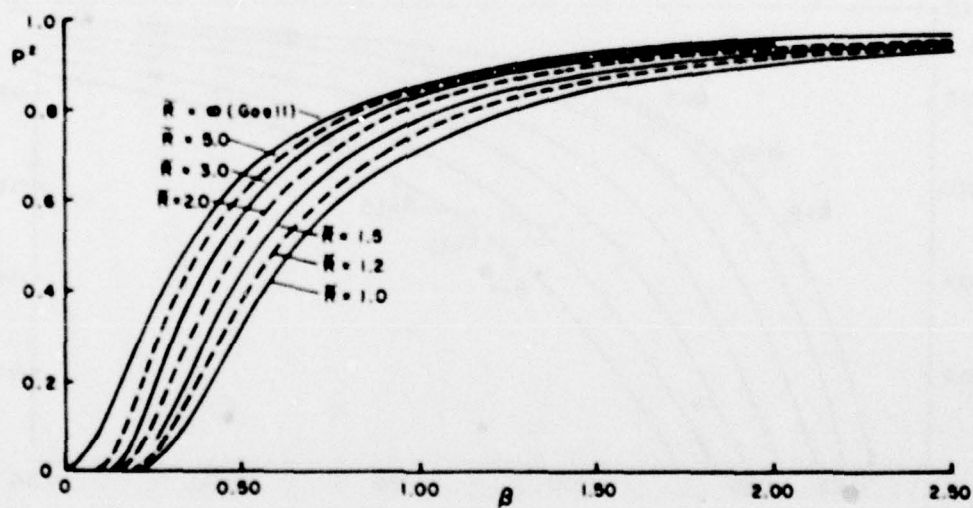


Figure 19. The R_1^I Mode of the Weakly Guiding Rectangular Guide as \tilde{R} Changes from 1 to ∞

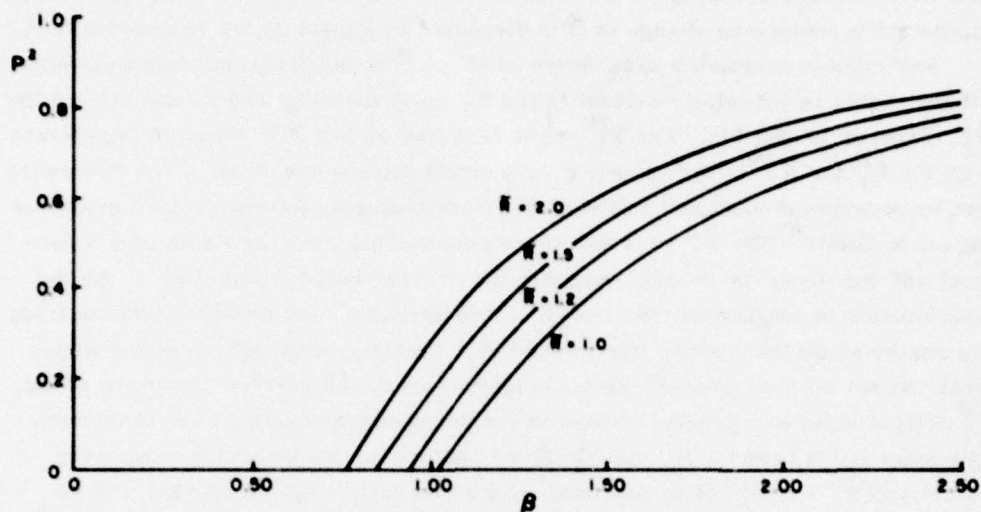


Figure 20. The R_I^{III} Mode of the Weakly Guiding Rectangular Guide as \tilde{R} Changes from 1 to 2

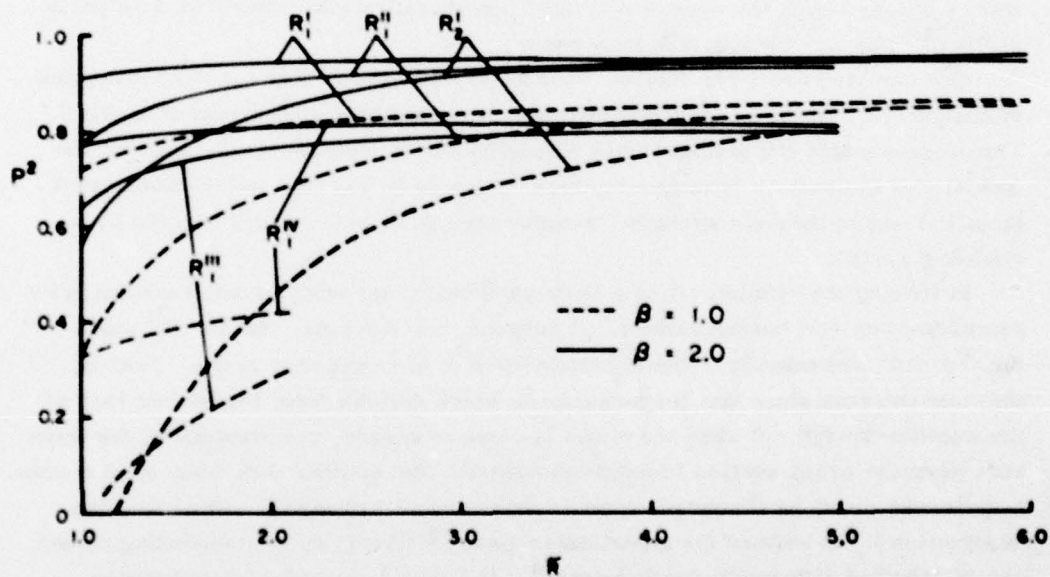


Figure 21. Variation of P^2 with Change in Aspect Ratio for the First Five Modes of the Weakly Guiding Rectangular Guide at Two Values of β

modes versus β for different rectangular cross sections, ranging from a square to an elongated rectangle. The behavior depicted here is typical of all modes in that cutoff occurs at smaller β as \tilde{R} increases. The evolution of these same five modes for a continuous change in \tilde{R} is displayed in Figure 21 for two values of β .

For certain modes the dependence of P^2 on \tilde{R} is much stronger than for most others. This is especially evident in the R_2^I mode (see Figures 16 and 21) and the R_1^{II} (Figures 17 and 21). The R_1^{IV} mode (Figures 18 and 21), which is degenerate with the R_1^{II} for $\tilde{R} = 1$, shows only a very small dependence on \tilde{R} . This difference can be understood when one refers to the field diagrams for the various modes as shown in Goell.² The R_1^{II} field has two maxima along the x-axis (the long direction) and one along the y-axis, whereas the reverse holds true for R_1^{IV} . As the x-dimension is lengthened, the two R_1^{II} lobes spread a considerable distance from the center along the x-axis, whereas the R_1^{IV} maxima, although squeezed somewhat, do not shift so dramatically. In other words, the greater distortion of the R_1^{II} field results in a greater change in the propagation constant as \tilde{R} increases. The same holds true for R_2^I and R_3^I (three maxima in one direction, one in the other) and R_3^{II} and R_3^{IV} (four and one). As a contrast, Figures 19, 20, and 21 display examples of moderate dependence on \tilde{R} , as evidenced by the R_1^I and R_1^{III} modes, respectively. In Figure 21 one can see much more vividly such effects as the splitting of the degeneracy in the R_1^{II} - R_1^{IV} mode as the cross section departs from a square, and, the crossing of the R_2^I propagation constant curve with those of the R_1^{III} and R_1^{IV} modes as \tilde{R} increases.

One can also see from figures such as 17, 19, and 21 that for very elongated rectangles ($\tilde{R} \geq 5$) the propagation constant is independent of \tilde{R} except at small β . This suggests that the greatest field strengths occur near the center and that the intensity at the ends is considerably less. This is indeed true except near cutoff (small β) where the field spreads throughout the guide and extends into the surrounding region.

In tracing the "evolution" of a mode as \tilde{R} increases one can avoid confusion by examining the field configurations. It happens, for example, that the R_2^{II} mode for $\tilde{R} \leq 1.2$ corresponds to the R_3^{II} mode for $\tilde{R} \geq 1.5$, and vice versa. That is, the field patterns show that the same mode which derives from the second root of the equation $\det(G) = 0$ when the shape is close to square, corresponds to the third root when the cross section becomes elongated. Put another way, individual modes may "cross over" as \tilde{R} changes (just as they may as β changes). However, the designation R_n^X is defined for a particular guide (\tilde{R} fixed), so corresponding modes can be labelled differently for different \tilde{R} . In Table 5 a similar circumstance occurs for ellipses.

For the first mode of each family (namely R_1^X) we find that the series converges nearly as well for large aspect ratios ($\tilde{R} \sim 10$) as for cases with \tilde{R} close to unity,

and four-term truncation provides reasonable accuracy for the second modes as well. However, for the higher modes of each family, 5, 6, and even 7 terms were required before the values of P^2 would be obtained to within 0.03 for such elongated cross sections.

Figure 22 exhibits the same information for the ellipse as was displayed in Figure 21 for the rectangle. As before, one can see how sensitive each mode is to change in aspect ratio, and, how a mode (for example, the $E_1^{\text{II}}-E_1^{\text{IV}}$) which is degenerate for a circular ($\tilde{R} = 1$) cross section splits as the cross section becomes elliptical.

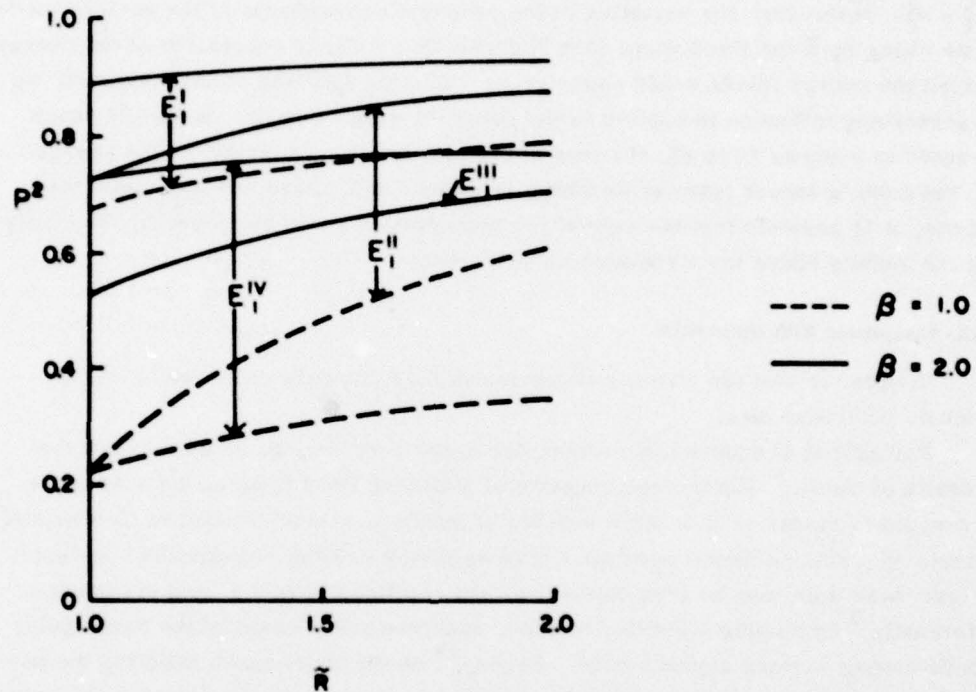


Figure 22. Variation of P^2 with Change in Aspect Ratio for Some of the First Few Modes of the Weakly Guiding Elliptical Guide at Two Values of β

Figures 16 to 22 demonstrate how different modes are affected by a change in the aspect ratio (\tilde{R}) for a fixed rectangular or elliptical shape. This was accomplished by keeping N constant in Eq. (60) and varying \tilde{R} . Of course, similar types of analyses could be carried out for changes in shape (N) as the aspect ratio remains fixed.

It is well known that the problem of finding the propagation constants of a waveguide having a particular geometry is identical to the problem of finding the energy levels of a quantum mechanical potential well whose potential has the same geometry as the waveguide. The Helmholtz equation inside the well, given by $(\nabla_1^2 + |V| - |E|)\psi = 0$, where $|V|$ is the well depth, $|E|$ is the energy level depth and ψ is the wave function, is the quantum mechanical counterpart of our Eq. (2). The Helmholtz equation outside the well, given by $(\nabla_1^2 - |E|)\psi = 0$, is the quantum counterpart to our Eq. (3). Thus, for the cases considered here, there is a one-to-one correspondence between the appropriate component of the electromagnetic field (E , B_z or Φ) and the quantum wave function (ψ), between $|V| - |E|$ and $\gamma_1^2 = k_1^2 - k_g^2$, between $|E|$ and $\gamma_2^2 = k_g^2 - k_2^2$, and between $|V|$ and $\gamma_1^2 + \gamma_2^2 = k_1^2 - k_2^2$. Moreover, the variation in the propagation constants of the various modes with changing \tilde{R} but fixed shape (see Figures 16 and 22) is suggestive of the changes which the energy levels would experience, including splitting of degeneracies, as a perturbing influence is applied to the potential well. For the waveguide cases treated in Figures 16 to 22, the role of the perturbation is played by the changes in the guide's aspect ratio as its shape remains fixed. Also, as was mentioned above, it is possible that the role of the perturbation could be played by the changes in the guide's shape for a constant aspect ratio.

8.5. Comparison With Other Work

In order to test the efficacy of our method we compare our results with previously published data.

For guides of square and rectangular cross sections, there are mainly the results of Goell.² His method consists of matching field components across the waveguide boundaries at a large number of points and then, similar to our method, obtaining a determinantal equation whose solutions are the propagation constants. From these solutions he then determines the coefficients in his field expansions. Marcatili,³ employing a similar method, analyzes a few cases of the rectangular guide having various aspect ratios. Eyges,¹² on the other hand, utilizing the perturbation techniques mentioned in Section 6, investigates some of the lower modes for guides having small values of \tilde{R} . Both authors report data which are in general agreement with Goell.

Some of Goell's results from the first six modes are shown in Figure 3 for the square and in Figure 6 for the $\tilde{R} = 2$ rectangle. They were taken as carefully as possible from his Figures 16 and 17 (square and $\tilde{R} = 2$ rectangle, respectively), taking note of the fact that his β differs from ours by a factor of 2. Also in Figure 6 we show the results from the perturbation prescription for the dominant (R_1^I) mode of the $\tilde{R} = 2$ rectangle. (It turns out that the latter method predicts values of P^2 for the dominant mode equal to those of a circular guide of the same

area). For the dominant mode ($E_1^{x,y}$ in Goell's notation) there is no discernible difference between his curve and ours, and only small differences for the perturbation analysis results. For several other modes there are nearly uniform differences of less than 0.07 in P^2 between Goell's results and ours. That is, the curves are adjacent and parallel, and certainly correspond to each other. For the square guide, the same type of results have also been found.

Many qualitative features which can be seen in our Figures 3 and 6 — such as the splitting of R_2^I and R_3^I (square) near cutoff and the crossing of R_1^{IV} and R_2^I (rectangle) — are also present in Goell's curves, although there are numerical discrepancies. Only with the R_{12}^{III} ($E_2^{x,y}$) mode of the rectangle are there discrepancies greater than 0.1 in P^2 .

With the square guide, all the odd modes are degenerate in pairs (sine and cosine) because of symmetry. (See Figure 3 and Table 2.) Moreover, except for R_1^I and R_1^{III} , those even modes in which the first term dominates are degenerate in pairs away from cutoff. This can be seen clearly in Figure 3 for the R_2^I - R_3^I modes. Furthermore, if the β -axis were extended to larger values, then this degeneracy would be more apparent for the R_2^{III} - R_3^{III} modes, as well as for higher modes which are not shown.

As a result of the foregoing, one could take a linear combination of the field expansions for two of these modes and derive an intensity pattern corresponding to neither of the individual modes, but rather to the combination. In fact, with our technique this would automatically occur if one did not recognize the simplifications implied by the symmetry and therefore effect the separation of the field expansions at the beginning. In Goell's Figure 5, intensity patterns for those modes which are degenerate reflect this combination of what appear — especially for the even indices — to be distinct modes. For rectangular cross sections ($\tilde{R} > 1$) our field intensity patterns agree with Goell's (see his Figure 6).

For guides of circular cross section, there are the works of Gloge¹ and Yeh.¹⁷ All of our results for this cross section agree very well with theirs. Yeh, however, also reports data for guides of elliptical cross section. A comparison of our results with his was frustrated by what may be either notational difficulties or a real discrepancy. The problem is that Yeh lists what appear to be two different, but degenerate, modes for the circular guide: ${}_e\text{HE}_{11}$ and ${}_o\text{HE}_{11}$ in his notation. Then, as the circle deforms into an ellipse, he shows each of these modes becoming a nondegenerate mode, with the propagation constants of one mode being greater in magnitude than those of the circular guide and those of the other mode being less. However, as can be seen in Figure 22, we find just one dominant mode (E_1^I) for the circle which does not split into two modes as \tilde{R} increases. In addition, our results for this single noncutoff mode agree very well with a

17. Yeh, C. (1976) Opt. and Quant. Elect. 8:43.

perturbation calculation based on Eyges.¹² Furthermore, Yeh's data for an elliptical guide having an aspect ratio of 2.164 do not correspond at all to our results for either an $\tilde{R} = 2$ ellipse (plotted in Figure 12) or an $\tilde{R} = 2.164$ ellipse. Hence, we are unable to correlate our results with his.

In view of the fact that our results for the rectangle and square agree quite closely with those of Goell and the fact that his point-matching method requires the evaluation of a determinant of order $4N$, with $3 < N < 9$, the economy of our method becomes obvious. Furthermore, unlike the differential equation approach utilized by Goell, our integral representation technique avoids the necessity of having to use a coordinate system dictated by the guide's cross-sectional shape as well as the special functions characteristic of that system. This means that in the case of the elliptic guides, for example, one need not be forced to use elliptic cylinder coordinates nor the complicated Mathieu functions associated with such coordinates.

9. CONCLUSION

The objectives of this paper have been (1) to present a general method by which the equations for the propagation constants of fiber waveguides of arbitrary cross sectional shapes may be written in a form suitable for efficient computation; (2) to specialize the method for weakly guiding fibers; and (3) to present limited results for the latter case to demonstrate the correctness and efficiency of the approach. The extension of this technique to coupled waveguides is currently in progress.

References

1. Gloge, D. (1971) Appl. Opt. 10:2252.
2. Goell, J. E. (1969) Bell Sys. Tech. J. 48:2133.
3. Marcattili, E. A. J. (1969) Bell Sys. Tech. J. 48:2071.
4. Marcuse, D. (1974) Theory of Dielectric Optical Waveguides, Academic Press, N. Y.
5. Kapany, N. S. and Burke, J. J. (1972) Optical Waveguides, Academic Press, N. Y.
6. Eyges, L. (1973) Ann. Phys. 81:567.
7. Love, J. D. and Snyder, A. W. (1977) Ann. Telecommunications 32:109;
di Vita, P. (1977) Ann. Telecommunications 32:115.
8. Eyges, L. and Gianino, P. D. (1979) IEEE Trans. Ant. & Prop.
AP-27:557.
9. Nelson, A. E. and Eyges, L. (1976) J. Opt. Soc. Am. 66:254.
10. Eyges, L. and Nelson, A. E. (1976) Ann. Phys. 100:37.
11. Waterman, P. C. (1969) J. Acoust. Soc. Am. 45:1417 and (1971) Phys. Rev.
D3:825.
12. Eyges, L. (1978) Appl. Opt. 17:1673.
13. Allard, J. (1964) Math. Mag. 37:210.
14. Gardner, M. (1965) Sci. Am. 213:222.
15. Hildebrand, F. B. (1956) Introduction to Numerical Analysis, McGraw Hill,
N. Y., p 330.
16. Hornbeck, R. W. (1975) Numerical Methods, Quantum Publishers, N. Y.,
p 65.
17. Yeh, C. (1976) Opt. and Quant. Elect. 8:43.